Monte-Carlo Simulation of Hard Spherocylinders under Confinement

Dissertation

zur Erlangung des Grades
"Doktor der Naturwissenschaften"
am Fachbereich Physik der
Johannes Gutenberg-Universität
Mainz

vorgelegt von
Yulia Trukhina
geboren in Moskau

Mainz, 2009

Tag der Prüfung: 16. Juli 2009

Zusammenfassung

Sobald ein Flüssigkristall auf eine Hohlraumgeometrie eingeschränkt wird, unterliegt das zugehörige Direktorfeld dem Zusammenspiel zweier Kräfte: Auf der einen Seite beeinflusst die Oberflächenkrümmung des Hohlraums das Direktorfeld ("Oberflächenverankerung"), wohingegen auf der anderen Seite diese Deformierung elastische Energie kostet. Das Direktorfeld wird im Gleichgewicht durch das Wechselspiel zwischen Oberflächenverankerung und Elastizität festgelegt. Ein typisches Beispiel für einen auf eine solche Geometrie eingeschränkten Flüssigkristall, welchem besonderes Interesse seitens der Physik zukommt, sind nematische Tröpfchen.

In dieser Arbeit wird ein System harter Stäbchen als eines der einfachsten Modelle für längliche Moleküle, aus denen nematische Flüssigkristalle aufgebaut sind, aufgefasst. Zunächst werden Systeme harter Spherozylinder innerhalb einer Kugel unter Verwendung von Monte Carlo Simulationen im kanonischen Ensemble untersucht. Im Gegensatz zu bereits existierenden simulationstechnischen Untersuchungen finden die Simulationen dieser Arbeit im Kontinuum statt. Insbesondere werden im Regime geringer Dichten Effekte der Ordnung in der Nähe harter, gekrümmter Wände studiert. Bei Zunahme der Dichte bildet sich zunächst ein uniaxialer Oberflächenfilm und bei weiterem Ansteigen der Dichte ein biaxialer Oberflächenfilm, welcher den ganzen Hohlraum ausfüllen kann. Wir untersuchen wie die Ordnung, die Adsorption und die Form des Direktorfeldes nahe der Oberfläche von deren Krümmung abhängen. Während die Orientierungsordnung an einer gekrümmten Wand des Hohlraums verstärkt wird im Vergleich mit einer ebenen Wand, ist die Adsorption schwächer. Im Fall von Dichten jenseits des isotrop-nematischen Phasenübergangs finden wir immer bipolare Konfigurationen.

Im weiteren Verlauf wird eine Erweiterung des Asakura-Oosawa-Vrij Modells für Kolloid-Polymer Mischungen auf anisotrope Kolloide verwendet. Mittels Computer Simulationen untersuchen wir, wie Tröpfchen harter, stäbchenförmiger Teilchen ihre Form und ihre Struktur unter dem Einfluss des osmotischen Drucks, welcher durch kugelförmige Teilchen hervorgerufen wird, ändern. Unter entsprechend hohem osmotischem Druck, richten sich die Stäbchen, welche Tropfen bilden, spontan aus, sodass uniaxiale nematische Flüssigkristalltröpfchen entstehen. Diese nematischen Tröpfchen oder "Taktoide" sind nicht kugelsymmetrisch, sondern länglich, was vom Wechselspiel der anisotropen Oberflächenspannung und der elastischen Deformation des Direktorfeldes herrührt. In Übereinstimmung mit jüngsten theoretischen Vorhersagen, stellen wir für ausreichend kleine Taktoide ein homogenes Direktorfeld fest, wohingegen große Taktoide durch ein bipolares Direktorfeld charakterisiert sind. Auf Grund von Veränderungen der Form und des Direktorfeldes der Tröpfchen, ergibt sich die Möglichkeit die Stärke der Oberflächenverankerung abzuschätzen.

Abstract

When a liquid crystal is confined to a cavity its director field becomes subject to competing forces: on the one hand, the surface of the cavity orients the director field ("surface anchoring"), on the other hand deformations of the director field cost elastic energy. Hence the equilibrium director field is determined by a compromise between surface anchoring and elasticity. One example of a confined liquid crystal that has attracted particular interest from physicists is the nematic droplet.

In this thesis a system of hard rods is considered as the simplest model for nematic liquid crystals consisting of elongated molecules. First, systems of hard spherocylinders in a spherical geometry are investigated by means of canonical Monte Carlo simulations. In contrast to previous simulation work on this problem, a continuum model is used. In particular, the effects of ordering near hard curved walls are studied for the low-density regime. With increasing density, first a uniaxial surface film forms and then a biaxial surface film, which eventually fills the entire cavity. We study how the surface order, the adsorption and the shape of the director field depend on the curvature of the wall. We find that orientational ordering at a curved wall in a cavity is stronger than at a flat wall, while adsorption is weaker. For densities above the isotropic-nematic transition, we always find bipolar configurations.

As a next step, an extension of the Asakura-Oosawa-Vrij model for colloid-polymer mixtures to anisotropic colloids is considered. By means of computer simulations we study how droplets of hard, rod-like particles optimize their shape and structure under the influence of the osmotic compression caused by the presence of spherical particles that act as depletion agents. At sufficiently high osmotic pressures the rods that make up the drops spontaneously align to turn them into uniaxial nematic liquid crystalline droplets. The nematic droplets or "tactoids" that so form are not spherical but elongated, resulting from the competition between the anisotropic surface tension and the elastic deformation of the director field. In agreement with recent theoretical predictions we find that sufficiently small tactoids have a uniform director field, whilst large ones are characterized by a bipolar director field. From the shape and director-field transformation of the droplets we estimate the surface anchoring strength.

Work is only then joyful when it is undoubtedly needed.

Lev N. Tolstoy

This thesis is based on the following publications:

- Yu. Trukhina and T. Schilling.

  Computer simulation study of a liquid crystal confined to a spherical cavity.

  Phys. Rev. E **77**, 011701 (2008).

- Yu. Trukhina, S. Jungblut, P. van der Schoot and T. Schilling.

  Osmotic compression of droplets of hard rods: A computer simulation study.

  J. Chem. Phys. **130**, 164513 (2009)

Contents

Chapter 1

Introduction

1.1 What are colloids?

A colloid or a colloidal dispersion consists of tiny particles or droplets dispersed in a continuous phase (solvent). The linear size of these particles varies from about hundred nanometres up to a few micrometres. The term "colloid" is usually used for both the substance itself and for the particles, which are dispersed in it. Its origin comes from a Greek word for a glue, so "colloid" means "glue-like". It was first introduced in 1861 by Tomas Graham to describe "pseudosolutions" in aqueous systems of silver chloride, sulfur, and Prussian blue which were prepared by Francesco Selmi in the nineteenth century [1]. These systems were characterized by a lack of sedimentation under the influence of gravity and had a low rate of diffusion. Graham concluded that the studied substance is a suspension of particles in a liquid medium and the particles have to be at least 1 nanometer in diameter but not larger than 1 micrometer.

Why are colloids so interesting and important? One of the possible answers is: Classical chemistry and physics use relatively small molecules with a molecular weight up to 10000. Polymer chemistry is using molecules with a molecular weight three orders of magnitude

higher. On the other hand, solid state physics is interested in the properties of condensed matter. Between these two scientific areas is the world of colloid chemistry. Colloid chemistry is closing the gap between molecular chemistry and solid state properties. Colloid chemists may use six orders of magnitude of molecular weight exclusively, including all the corresponding effects. Some people name this region as "mesoscopic", since the colloidal region is located in between well known scientific length scales.

There are several types of forces that govern interactions of particles inside a colloidal substance. All play an important role, though not necessarily on the same length scale and in the same way. Some may help stabilize a colloid while others may do the opposite.

The simplest is the excluded volume force. It is a repulsive force which is present due to the fact that two hard particles cannot overlap.

Often an important force is the electrostatic force, as usually some charge is adsorbed to the surface of the particles in a colloid. All particles adsorb a like charge so they repel. This force helps stabilizing the colloid. Because the surface of colloidal particles is so great compared to their mass, the interaction due to their surface charge can overcome their kinetic energy and the particles will not come close to each other.

Colloidal particles may have permanent electric dipole moments, or such moments can be temporarily present because of the fluctuating electric charge density. Such temporary dipoles will induce a dipole moment in particles in the vicinity as well. The two particles, dipoles, will attract - the force between them is the van der Waals force. If the van der Waals forces prevail in a colloid, the particles inside it will tend to aggregate and ultimately settle on the bottom or on the surface of the substance.

Steric forces between particles may create a repulsive or an attrac-

tive effect. The surface of particles covered with certain polymers or the dispersing mediums made of polymers that don't adsorb on the particles dispersed in it can cause such interaction. These two possible cases are the so called steric stabilization or the attractive depletion force.

Brownian forces (diffusion) on individual particles also play a role, as they must overcome gravity and buoyancy and cause the dispersed particles to move in random directions. For instance, brownian forces prevent full sedimentation of colloids under the influence of gravity.

In this work we investigate the model of colloids in which only the excluded volume force is present, in other words it is entropy that determines what kind of ordering appears in the system. Running a step forward, one can say that there are positional and orientational contributions to entropy in case if the system is formed of particles, whose shape is different from a spherical one; both these contributions lead to a complex phase diagram.

1.2 Non-spherical colloids

Colloids can have different shape, for instance, clay consists of platelets, red blood cells are toroidal, tobacco mosaic virus (TMV) and fd viruses have a rodlike shape (see Figure 1.1 and Figure 1.2 respectively). In this work we focus on hard-rod fluids, i.e., fluids of elongated particles that interact via a harshly repulsive excluded-volume interaction potential, which are very immensely useful as a model system for investigating the formation, structure and properties of liquid crystals [2]. The term "liquid crystal" refers to substances which have properties between those of simple liquids (which are composed of spherically symmetric particles), and those of a solid crystal. The coupling between orientational and positional degrees of freedom

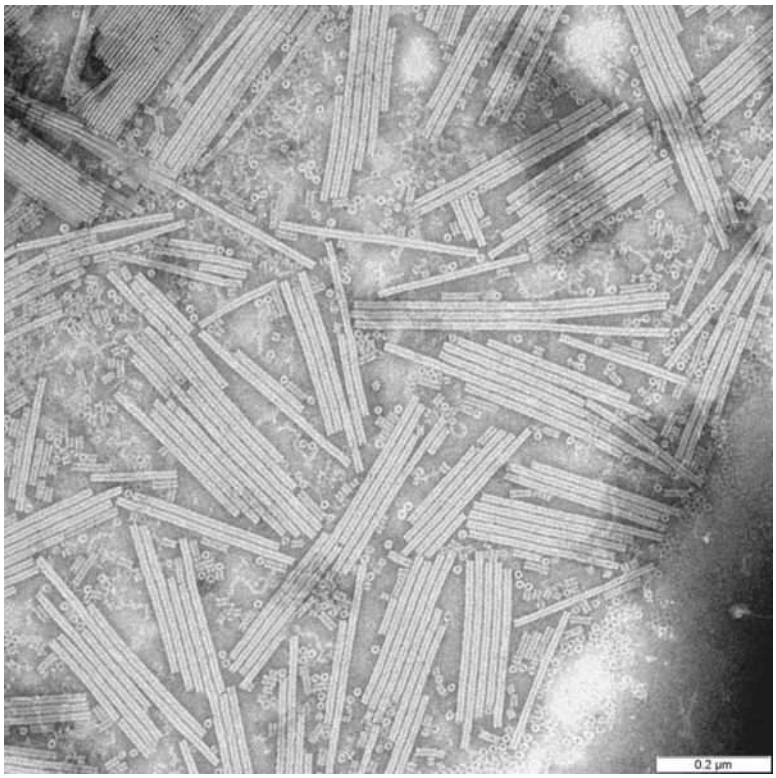

Figure 1.1: An electron micrograph of a tobacco mosaic virus. Source: http://en.wikipedia.org/wiki/User:Xmort.

leads to a large variety of phases. Anisotropic particle shapes and anisotropic interactions between the particles, from which the material is formed, are the origin of this.

Closest experimental realizations of the hard-rod fluid model are found in fluid dispersions of very stiff polymers, inorganic rod-like colloids, filamentous viruses, fibrillar or tubular protein assemblies, and carbon nanotubes [3, 4, 5, 6, 7].

Fluids of rodlike particles have attracted much attention over the years. Experimental observations date back to the 1920s and 1930s, when Zocher [8] and Bawden et al. [9] investigated systems of tobacco mosaic virus particles, and found a phase transition from an isotropic fluid phase at low concentrations to an orientationally ordered nematic

Figure 1.2: An electron micrograph of an fd virus, the contour length is equal to 880 nm, the diameter is equal to 7 nm. Source: http://www.rowland.harvard.edu/rjf/dogic.

phase at higher concentrations. The latter phase is characterized by long-range orientational ordering of the particles. However, there is no translational ordering: i.e. there are no long-range positional correlations of the centers of mass of the particles. In this phase the particles are aligned along a preferred direction while their spatial positions are, like in an ordinary liquid, homogeneously distributed in space. The preferred direction is called the nematic director. It can be macroscopically observed by illuminating a nematic sample between crossed polarizers.

This density-driven isotropic-nematic phase transition in a homogeneous bulk fluid of rodlike particles was considered theoretically in the 1940's by Onsager, who showed that an isotropic dispersion of hard infinitely long rods must undergo a first order orientational ordering transition when the density is sufficiently high [11]. We discuss this theory more detailed in Section 1.3.

At even higher densities the system of hard rods can transform into another liquid crystalline phase, called "smectic". This phase has not only orientational ordering but also some translational one - it also forms layers, in which the particles are still free to move, meaning that there is now translational order inside one layer - the system has long-range positional order only in one direction.

Eventually, at sufficiently high pressures, crystallization will take place, with long-range positional order in all three directions. We show

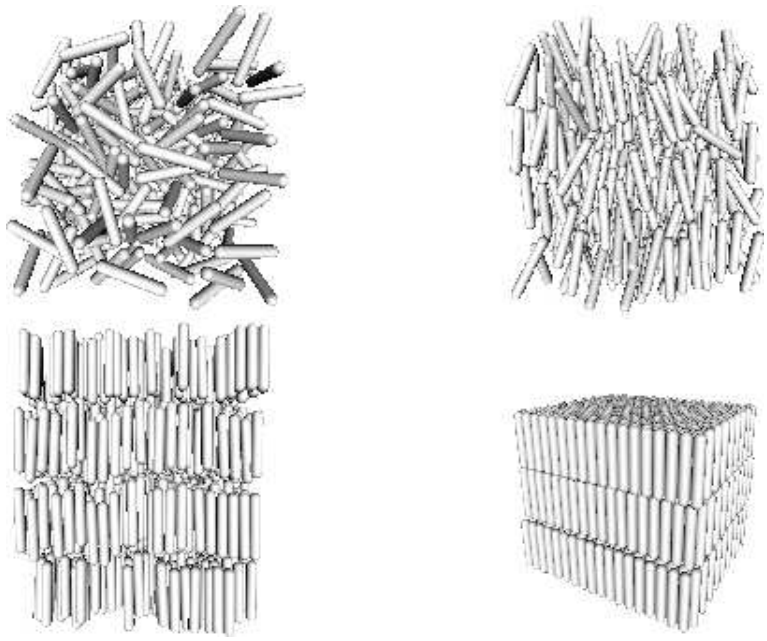

Figure 1.3: Sequence of phases of a system of hard spherocylinders [10]. Top left: the systems with lowest density form an isotropic phase, there is no translational and orientational ordering. Top right: higher density, the system forms a nematic liquid crystal with orientational ordering but without translational one. Bottom left: even higher density, the system forms a smectic liquid crystal with orientational ordering and translational ordering on one direction. Bottom right: at sufficiently high density the system forms a crystal phase with orientational and translational ordering in three directions.

schematically the sequence of this ordering in Figure 1.3 for the case of hard spherocylinders, which are a model for rodlike particles.

1.3 Onsager theory

A fluid of hard rods can be considered as the simplest model for nematic liquid crystals consisting of elongated molecules.

In the 1940s Onsager showed [11] that the transition between the isotropic phase (I) and the nematic phase (N) is of entropic nature and that it can be explained by simple geometrical arguments. He did

that by accounting for the IN transition in terms of a competition between the maximization of orientational entropy and minimization of excluded volume. A main part of Onsagers theory is the one-particle distribution as a function of the rod orientation, for which he derived a nonlinear integral equation. This equation is exact when the length-to-diameter ratio of the rods tends to infinity. At low bulk densities the only solution to this equation is a uniform constant, which describes the isotropic phase, while at sufficiently high densities a nonuniform solution of uniaxial symmetry exists, which describes the nematic phase. Although explicit calculation of these peaked nematic distributions is analytically intractable, this is numerically straightforward because the uniaxial symmetry reduces the problem to a onedimensional one in the polar angle of the rod orientation.

The steric hard-body interactions, taken into account in that work, already capture many of the essential features of liquid crystals, however their actual behaviour is complicated by the presence of the flexibility, dipole moments, etc. But for certain colloidal systems of rodlike particles of synthetic or biological origin dissolved in a suitable solvent, the hard body model provides a quantitatively reliable effective description [7]. Among them, the ones which are studied in most detail are the tobacco mosaic virus and the fd-virus with length to diameter ratios of about 17 and 150 respectively [7]. From a theoretical point of view the limit of infinitely thin hard rods is especially interesting because it represents one of the very few cases for which the exact density functional is known [11].

A first attempt to map out the phase diagram of hard spherocylinders with finite lengths L and diameter D was reported by Veerman and Frenkel [12]. However, this study focused on only a small number of rather widely spaced values of the aspect ratio L/D. As a consequence, the phase boundaries for intermediate values could only be sketched, while some phase boundaries were not studied at all. This

situation was clearly unsatisfactory, as the system of hard spherocylinders is now often used as a reference system to compare both with experiment and with theory. For precisely this reason, McGrother et al. [13] performed more extensive simulations in the region $3 < L/D < 5$.

Further investigations of the phase diagram of hard spherocylinders have been done by Bolhuis and Frenkel, in which they used computer simulations and Gibbs-Duhem integration [14], and by Graf and Löwen, who used the density functional theory [15]. A good agreement has been found between the results of the two approaches.

1.4 Liquid crystals under confinement

Technical interest in liquid crystalline materials confined to curved geometries is very strong because of their important role in electro-optic technologies [16]. The interest in confined systems of organized fluids significantly grew up after the discovery of the usefulness of these materials, especially in electrically controllable light scattering windows [17] and reflective mode display technology [18]. Independent of the method, that is used for confining liquid crystals, phase separation [19], encapsulation [20, 21], or permeation [22, 23], these systems have one underlying common feature: a non-planar confinement imposed by the surrounding substance. The interplay between the ordering interactions at the interface with the confining medium and the elastic deformation energies of the liquid crystal results in a variety of interesting effects. The most studied observables are changes in the nature of the nematic-isotropic transition [24, 25, 26], the specific director configuration inside the cavity [27, 28, 29, 30, 31, 32] and the variable angle at which the elongated molecule is anchored at the cavity wall [33, 32, 24, 25].

In addition to the breaking of the symmetry, one has to mention one

other important feature of confined liquid crystal systems - in contrast to microscopic bulk liquid crystals they have large surface-to-volume ratio.

Surface anchoring

Interactions with surfaces play a great role even in the case of simple liquids, while they induce density distortions in such systems. Even more than in simple liquids, surface effects are of great importance for liquid crystals, for which not only changes in density take place, but also orientations of the molecules can be influenced. Liquid crystals in contact with a solid substrate (or at interfaces with another medium) often adopt a preferred direction of alignment, this effect is called surface anchoring [34, 35, 36].

For a nematic liquid crystal three preferred alignments at the surface can been observed, i.e., the director can be oriented normal to the interface (homeotropic anchoring), parallel to the interface (planar or homogeneous anchoring), or along a tilted direction [35].

The most relevant for this work is the ideal case of a system of rods near a flat hard wall. What kind of surface anchoring appears in this case? Let us consider two opposite cases - parallel and perpendicular orientations. One can easily see that in the first case the system gains more free volume; this in turn leads to increasing of the entropy. Thus, parallel orientation is favoured (Figure 1.4). However, as it was already mentioned, for different geometries and properties of the wall/interface other types of anchoring can appear.

One has to mention, that the curvature of the wall can be a factor, that influences the ordering in the system. The curvature has an appreciable influence even on simple liquids, which are composed of spherically symmetric particles, changing their positional structure [37, 38]. In case if the fluid consists of elongated particles and the ra-

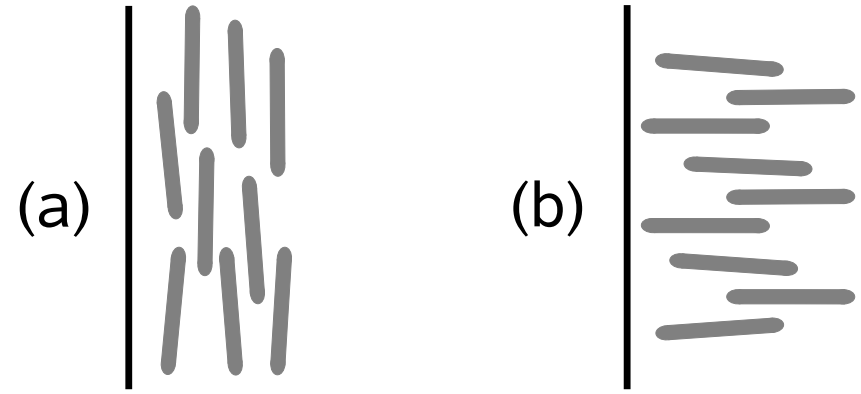

Figure 1.4: A schematic representation of a system of spherocylinders in a nematic phase near a flat hard wall with a a) planar anchoring, b) homeotropic anchoring.

dius of the curvature is not negligible, the orientational and positional order is changed comparing to the case of a flat wall [39, 40].

Elasticity

The elastic free energy for the nematic liquid crystal, called the Frank-Oseen free energy [41, 42], under certain assumptions can be defined as

$$F_{\mathrm{el}} = \frac{1}{2}\int d\vec{x}\,[K_{11}(\nabla\cdot\vec{n})^2 \;+\; K_{22}[\vec{n}\cdot(\nabla\times\vec{n})]^2 \;+\; K_{33}[\vec{n}\times(\nabla\times\vec{n})]^2, \tag{1.1}$$

where $\vec{n}$ is local the nematic director, K_{11}, K_{22}, and K_{33} are the elastic constants for splay, twist, and bend distortions, respectively. These different types of distortions are schematically shown in Figure 1.5.

In case of a liquid crystal one has a very soft system, in which elasticity plays a big role and thus has to be taken into account. Some investigations [43, 44] show that in case of liquid crystal droplets surface tension can have a very small value, because it's purely entropic. Because of the low value of the surface tension these droplets can be easily deformed. Thus, deformation really matters for such systems.

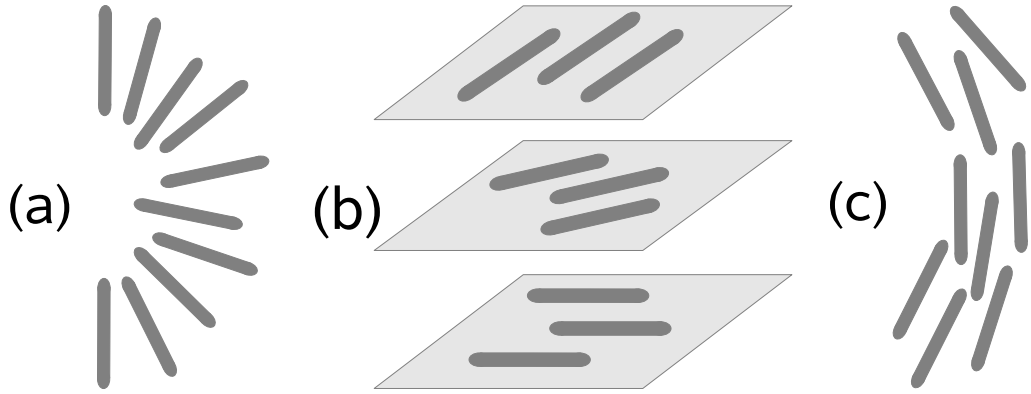

Figure 1.5: A schematic representation of different types of elastic distortions in a nematic system: a) a splay distortion, b) a twist distortion, c) a bend distortion.

So, one has to take elasticity into account (however, one has to mention that it is necessary to take into account elastic distortions in all systems with high surface anchoring).

The history of confined LC

The study of equilibrium structures and defects of liquid crystals under confinement has been an area of interest of many physicists and chemists for a long time.

One of the first investigations of confined liquid crystals was performed in the early 1900s when supramicrometre nematic liquid crystal droplets were successfully suspended in a viscous isotropic medium [45]. The birefringent textures were studied with optical polarizing microscopy, and it was concluded that the specific director configuration within the spherical confining cavity depends on the liquid crystal material and the angle at which the liquid crystal molecules are anchored to the isotropic fluid interface.

Much later, in the experimental studies Meyer [46] observed radial and bipolar configurations. At the same time Dubois-Violette and Parodi [27] applied the Frank-Oseen elastic theory [41, 42] to pre-

dict several stable nematic director-field configurations in spherical droplets. They showed the stability of the bipolar and radial nematic director fields under certain conditions. They also demonstrated that in the presence of an applied electric field for materials with a positive dielectric anisotropy the bipolar droplet reorients parallel to the electric field direction while the radial droplet experiences a configuration transition to the axial structure

In the early 1980s the liquid crystal droplet problem was re-examined from the basic standpoint. Volovik and Lavrentovich [33] extensively studied the dynamics of creation, annihilation and transformation of topological defects (e.g. boojums, hedgehog and disclinations) in a closed system following predictions of topological theory. Up to this point, the interest to confined liquid crystals was only due to the basic science perspective.

In 1982, Craighead and coworkers proposed a possible device which used confined liquid crystals as an electro-optic light valve, (in which a microporous membrane permeated with a positive dielectric anisotropy liquid crystal). In the absence of an electric field, the permeated membrane is slightly scattering because of the mismatch between the indices of refraction of the membrane and the liquid crystal. Upon application of an applied voltage, the ordinary index of refraction of the liquid crystal is closely matched to that of the microporous matrix, and the permeated membrane becomes transparent for light propagating along the field direction. The device proposed by Craighead et al. [22] was never commercialized because of inadequate contrast.

The usefulness of spherical nematic droplets became much more clear, when the middle-1980s it was discovered that submicrometre and micrometre droplets could easily be dispersed in a rigid polymer binder [19, 20, 21]. By matching the ordinary refractive index of the liquid crystal with that of the polymer binder, an electrically control-

lable light scattering medium transforms from a translucent, white appearance to a transparent appearance upon application of an applied voltage. The potential of polymer-dispersed liquid crystals in electro-optic light shutters revived the interest in liquid crystals confined to curved geometries.

1.5 Outline of the thesis

In this thesis, Chapter 2 describes the Metropolis Monte Carlo technique and the model of spherocylinders which are used in our simulations.

In Chapter 3, systems of hard spherocylinders in a spherical geometry are investigated. In particular, the effects of ordering near hard curved walls are described in Section 3.2 for the low-density regime. With increasing density, first a uniaxial surface film forms and then a biaxial surface film, which eventually fills the entire cavity. We study how the surface order, the adsorption and the shape of the director field depend on the curvature of the wall. Section 3.3 describes the ordering of spherocylinders in a nematic regime inside a hard cavity.

Chapter 4 decribes how droplets of hard spherocylinders optimize their shape and internal structure under the influence of the osmotic compression caused by the presence of spherical particles that act as depletion agents. At sufficiently high osmotic pressures the rods that make up the drops spontaneously align to turn them into uniaxial nematic liquid crystalline droplets. We investigate the shape and the inner structure of the obtained isotropic and nematic droplets and estimate the surface anchoring strength and an average of the elastic constants of the hard-rod nematic.

Chapter 2

Simulation method and model

2.1 The Metropolis Monte Carlo algorithm

As it was mentioned above, the molecular organization inside the droplets can be strongly influenced by varying the properties of the polymer outside and the preparation method, i.e. the boundary conditions at the droplet surface. This in turn influences the orientation of molecules near the surface and the aligning effect may propagate inside the droplet. In general there is a competition between the molecular orientation induced by the surface boundary conditions, the effects of ordering of the liquid crystal itself due to the molecules trying to arrange parallel to each other, and the disordering effect. The resulting molecular organization for a certain boundary condition depends on a number of factors. Thus, it is not easy to predict the actual molecular organization with available theories and even, especially for the smaller sizes, to investigate it experimentally. Due to this reason, performing computer simulations can be useful for investigating such problems.

Statistical mechanics relates macroscopic properties of matter to the microscopic description of the system. The fundamental quantity in statistical mechanics is the canonical partition function, which is

the sum of the Bolzmann factors over all possible states i of a system of N particles in a volume V at a fixed temperature T

$$Z = \sum_i e^{-E_i/k_BT}. \tag{2.1}$$

Here k_B is Boltzmann's constant, T is the absolute temperature, and E_i is the total energy of the system in state i. The Bolzmann's factors e^{-E_i/k_BT} are proportional to the probability of finding the system in state i. One therefore can calculate the average of an observable A as

$$\langle A \rangle = \frac{\sum_i A_i e^{-E_i/k_BT}}{Z}. \tag{2.2}$$

In classical mechanics, the states of the system are actually uncountable. This leads to the fact that 2.1 and 2.2 take a form of integrals over the phase space. In some particular cases these integrals can be calculated exactly, in all other cases one is left with two options: either one uses approximate analytical theories that simplify the integrals to the extent that they can be evaluated, or one can use numerical techniques, such as Monte Carlo or molecular dynamics simulations. In this work we present the results of the simulations performed using Monte Carlo methods, so we focus now on it.

The most simple Monte Carlo technique is random sampling. Applying this method to calculating 2.2 means placing N particles into a random configuration, evaluating E_i and giving this configuration the weight e^{-E_i/k_BT}, then repeating the procedure. The problem of this method is that generating random configuration leads to inefficient calculations, because the configurations that have small weight e^{-E_i/k_BT} are examined as often as configurations with a high weight. And this leads to the fact that the simulation time needed to calculate the observables with a good accuracy becomes enormous. One algorithm, which allows to solve this problem, was proposed in 1953 by Metropolis et al. [47]. The main idea of this method is to choose

configurations with a probability e^{-E_i/k_BT} and to weight them evenly, instead of choosing configurations randomly and weighting them with e^{-E_i/k_BT}, as was done before.

Then the average of A can be calculated as

$$\langle A \rangle = \frac{\sum_{k=1}^{M} A_k}{M}, \tag{2.3}$$

here M is the total amount of trial moves. In the rest of this work, "Monte Carlo" always refers to the Metropolis Monte Carlo algorithm.

2.2 Monte Carlo simulation of hard spherocylinders

Spherocylinders are an example of non-spherical particles. This means that when one uses the Metropolis-scheme one has to generate not only positional displacements but also orientational moves. In order to avoid biasing the system, the new (trial) orientations must be uniformly distributed in some solid angle around the previous ones. One can achieve this by, first, selecting a random vector which is uniformly distributed on a surface and, second, accepting this new vector if the angle between the new vector and the old one is smaller than a value, defined in the beginning of the simulation. One can perform the first step using several different mathematical methods. For example, one of the most simple and efficient methods is the one of von Neumann [48]:

- Generate x_1, x_2 and x_3 independently so that they are uniformly distributed on $(-1, 1)$.
- Calculate $S = x_1^2 + x_2^2 + x_3^2$. If S is larger than 1 repeat from the previous step.

- Form a vector $(x_1/\sqrt{S}, x_2/\sqrt{S}, x_3/\sqrt{S})$.

The idea of this method is to choose a point in a cube (step 1), reject it unless it is in the inscribed sphere (step 2), then project the point to the surface of the sphere (step 3).

The efficieny of the described method is $\pi/6$, so one needs to choose $18/\pi \cong 5.73$ uniformly distributed variables, on the average. A more efficient method was proposed in 1972 by George Marsaglia [49]. This method has an efficieny $\pi/4$, and one needs on average $8/\pi \cong 2.55$ uniformly distributed variables. This means that this method is approximately twice faster than the method which was described above, that's why we choose it in our simulations. The method consists of such steps:

- Generate x_1^0 and x_2^0 independently so that they are uniformly distributed on $(-1, 1)$.
- Calculate $S = (x_1^0)^2 + (x_2^0)^2$. If S is larger than 1 repeat from the previous step.
- Evaluate $x_1 = 2x_1^0\sqrt{(1-S)}$, $x_2 = 2x_2^0\sqrt{(1-S)}$ and $x_3 = 1 - 2S$.
- Form a vector (x_1, x_2, x_3).

In order to see that this method works one has to combine two facts:

1. If (x_1, x_2, x_3) is uniform on the surface of the unit 3D sphere, then each x is uniform on $(-1, 1)$ (the area of a spherical cap is a multiple of its height), and (x_1, x_2), for given x_3, is uniform on a circumference of the circle of radius $\sqrt{1 - x_3^2}$.
2. If (x_1, x_2) is uniform over the interior of the unit circle, then $S = x_1^2 + x_2^2 + x_3^2$ is uniform on $(0, 1)$ and independent of the point $(x_1/\sqrt{S}, x_2/\sqrt{S})$.

Another important aspect is that in Monte Carlo simulations of hard-particle fluids only those trial moves must be accepted that do not lead to overlaps of the particles, and otherwise they must be rejected. This means that if one wants to write an efficient simulation code one has to make the determination of the overlap between two particles as fast as possible. The simulations presented in this work are performed on a system consisting of hard spherocylinders, for which efficient and simple overlap criteria have been developed [50].

2.3 Model

Similar to Onsager's approach, we consider spherocylinders each consisting of a cylindrical part of length L and diameter D, capped at both ends by hemispheres of diameter D.

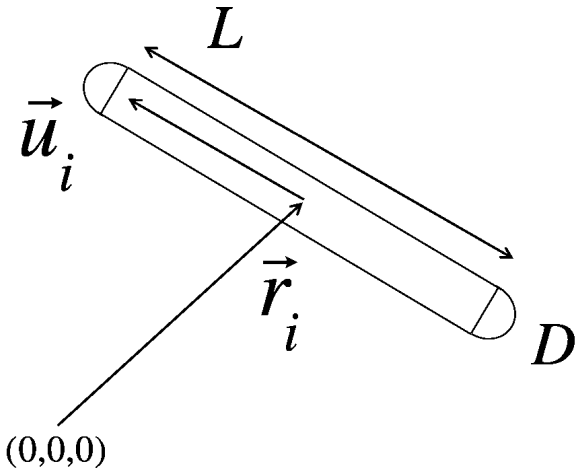

Figure 2.1: Sketch to introduce definitions: Each spherocylinder consists of a cylinder of length L and diameter D capped by two hemispheres of diameter D. The location of the i-th spherocylinder is given by its centre of mass vector $\vec{r}_i$ and the orientational unit vector $\vec{u}_i$.

The location of the i-th spherocylinder is given by its centre of mass vector $\vec{r}_i$ and the orientational unit vector $\vec{u}_i$ pointing along the long

axis of the particle (Figure 2.1).

The rod-rod interaction potential is hard:

$$U_{ij} = \begin{cases} \infty, & \text{if particles } i \text{ and } j \text{ overlap} \\ 0, & \text{otherwise.} \end{cases} \tag{2.4}$$

2.4 Tensor order parameter

In this work we are interested in investigating systems in isotropic and nematic phases. In the isotropic fluid phase, the orientations and positions of the molecules are disordered. In the nematic phase, the positions of the molecules are still disordered, but their long axes are oriented on average along a particular direction. Thus, the nematic phase is characterized by broken rotational but not translational symmetry. It is, therefore, tempting to associate the order parameter with the unit vector $\vec{u}_i$ which points along the long axis of the spherocylinder i. However, since the spherocylinders have equal probability of pointing parallel or anti-parallel to any given direction, any order parameter must be even in $\vec{u}_i$. Thus, we define the average alignment in terms of the orientational traceless tensor $\mathbf{Q}$ with the elements

$$Q_{\alpha\beta} = \frac{1}{2N_r} \sum_{i=1}^{N_r} \left(3u_{i\alpha}u_{i\beta} - \delta_{\alpha\beta}\right), \tag{2.5}$$

where $u_{i\alpha}$ is the α component ($\alpha = x, y, z$) of the unit vector along the axis of particle i, $\delta_{\alpha\beta}$ is the Kronecker delta, and N_r is the number of rods for which the order parameter is calculated. For obtaining reliable results one needs to take a large number of rods. However, making simulations for sufficiently large systems can be too time consuming, so one often investigates smaller systems. This order parameter can be

also used for analyzing them by making the average over uncorrelated configurations of such systems.

Diagonalization of the tensor yields three eigenvalues, λ_+, λ_0 and λ_-, where $\lambda_+ > \lambda_0 > \lambda_-$. The case $\lambda_+ > 0$, $\lambda_0 = \lambda_-$ corresponds to a structure with one preferred direction. The case $\lambda_+ = \lambda_0 > 0$ corresponds to a structure in which one direction is avoided and the two other directions are equally favoured. All the intermediate cases $\lambda_+ > 0$, $\lambda_+ > \lambda_0 > \lambda_-$ correspond to a biaxial structure. And in an isotropic phase one finds $\lambda_+ = \lambda_0 = \lambda_- = 0$ (in an infinitely large system).

Various authors use different definitions of the nematic and biaxial order parameters [51, 52] (for instance, the nematic order parameter can be defined either as a largest eigenvalue or as an eigenvalue with the largest absolute value, thus, leading to completely different results for the systems with two equally favoured directions). To avoid confusion about the nematic order parameter, we plot the relevant eigenvalues instead. To detect biaxial order, we use $\Delta = \lambda_+ - \lambda_0$.

Biaxiality effects in the system of hard spherocylinders become pronounced in confinement, where the walls (or interfaces) introduce ordering (e. g. parallel or perpendicular to them).

2.5 Symmetry and averaging

Depending on the structure there can be different types of symmetry in the system. When calculating observables, such as the components of order parameter tensor, properly averaged over the ensemble of configurations, all of them have to be taken into account. In the case of radial symmetry we calculated the orientational tensor directly by averaging over all configurations obtained in the simulations.

However, one has to proceed differently if there is an axis in the

system along which the particles tend to align. As rotations of the overall director do not cost any (free) energy, the orientation of this axis can fluctuate strongly during a simulation run.

In order to average some local properties of interest the configurations need to be rotated in such a way that the director always points in the same direction. (Note that this does not imply that we rotate the system during the simulation, this is done afterwards during the analysis of the configurations.) This procedure introduces a small systematic error to the computation of the orientational order parameters, which is negligible in the context of the analysis presented in chapters 3 and 4.

In order to do that we calculate the orientational tensor $\mathbf{Q}$ for all the particles in a given configuration. The eigenvector $\vec{v}_+$ corresponding to the largest eigenvalue λ_+ gives the orientation of the nematic director field. And then we rotate the configuration in such a way that the z-axis aligns with the orientation of the vector $\vec{v}_+$:

1. First, we rotate the system around the z-axis by means of multiplying all the centre of mass vectors $\vec{r}_i$ and the orientational vectors $\vec{u}_i$ by a rotational matrix T_z

$$\vec{r}_i\prime = T_z\vec{r}_i = \begin{pmatrix} \cos\varphi & -\sin\varphi & 0 \\ \sin\varphi & \cos\varphi & 0 \\ 0 & 0 & 1 \end{pmatrix} \begin{pmatrix} r_x \\ r_y \\ r_z \end{pmatrix}, \tag{2.6}$$

   where φ is determined as an angle between the y-axis and the projection of the vector $\vec{v}_+$ to the xy-plane, so,

$$\sin\varphi = \frac{v_+^y}{\sqrt{(v_+^x)^2 + (v_+^y)^2}}. \tag{2.7}$$

   The result of this operation is that the x-component of $\vec{v_+}$ becomes equal to 0 after rotation: $v_+^x\prime = 0$.

2. Second, we rotate the system around the x-axis by means of multiplying all the centre of mass vectors $\vec{r}_i\prime$ and the orientational vectors $\vec{u}_i\prime$ obtained in step 1 by a rotational matrix T_x

$$\vec{r}_i\prime\prime = T_x\vec{r}_i\prime = \begin{pmatrix} 1 & 0 & 0 \\ 0 & \cos\theta & -\sin\theta \\ 0 & \sin\theta & \cos\theta \end{pmatrix} \begin{pmatrix} r_x\prime \\ r_y\prime \\ r_z\prime \end{pmatrix}, \tag{2.8}$$

where θ is determined as the angle between the z-axis and the vector $\vec{v}_+$, so,

$$\sin\theta = \frac{v_+^z}{|\vec{v}_+|}. \tag{2.9}$$

The result of this operation is that the y-component of $\vec{v_+}$ becomes equal to 0 after rotation: $v_+^y\prime\prime = 0$, $v_+^x\prime$ remains equal to 0, $v_+^x\prime\prime = 0$, and v_+^z becomes equal to $|\vec{v}_+|$.

In the rest of this work we use r instead of $r\prime$ and $r\prime\prime$ for simplicity.

If there is a cylindrical symmetry around the z-axis and a top-down symmetry with respect to the $(x-y)$ plane, then the particles can be interpreted as lying with their centres on a quarter of a circle with the coordinates $r_{xy} = \sqrt{r_x^2 + r_y^2}$ and $|z|$ (in the following text we use z instead $|z|$ for simplicity).

In order to obtain spatially resolved information about the system the simulation sphere is divided into bins of equal volume. We denote the number of particles in such a bin as $N(r_{xy}, z)$. The orientational tensor $\mathbf{Q}$ is then accumulated in these bins over all the equilibrated conformations and only then the eigenvalues are calculated (the biaxial order parameter accordingly). For the density the order of averaging does not change the result.

2.6 Cell-system

One of the most important things in computer simulation is the speed of the execution of the program. In case of simulating the fluid of hard spherocylinders in the NVT-ensemble the most "time-expensive" part of the code is the procedure of detecting of overlaps between spherocylinders. One could significantly simplify this procedure if the closest neighbours to the particles were known. This can be done by discretization of the space, namely, dividing the simulation box into cubic cells. An important question arises then - which cell size to choose? Of course, the one which is equal (or larger) to the rod length is the easiest for implementation. However, for long spherocylinders such a discretization is not efficient enough. A way to introduce a cell system with smaller cells was proposed in [53]. This method allows to make the cells as small as the diameter of the spherocylinders.

Chapter 3

Rods in spherical geometry

When a liquid crystal is confined to a cavity its director field becomes subject to competing forces: on the one hand, the surface of the cavity orients the director field ("surface anchoring"), on the other hand deformations of the director field cost elastic energy. Hence the equilibrium director field is determined by a compromise between surface anchoring and elasticity. One example of a confined liquid crystal that has attracted particular interest from theoretical physicists is the nematic droplet. A nematic droplet inside a liquid surrounding (e. g. the coexisting isotropic phase or a polymer matrix) can not only adapt its director field but also its shape. Various authors have discussed the morphologies of nematic droplets in the framework of Frank elastic theory and Landau-de Gennes theory [54, 27, 31, 55]. In particular, Prinsen and van der Schoot have recently given a detailed analysis of this problem [56, 57, 58].

Inspired by the development of polymer dispersed liquid crystal displays, the properties of nematic droplets have also been studied in experiments and simulations [25, 59, 60]. In particular, Zannoni and coworkers performed several computer simulation studies of the Lebwohl-Lasher model inside a spherical cavity [61, 62, 63, 64, 65, 66, 67, 68]. In this model the positional degrees of freedom are discretized,

while the orientations vary continuously. The results, which we show in section 3.3, agree well with their results.

The bulk phase behaviour of hard spherocylinders is well known [14, 69, 15]. Less is known, however, about the effect confinement has on this model. Hard spherocylinders in contact with a planar hard wall have been studied within the Onsager approximation, i. e. for infinite aspect ratio, by Poniewierski and Hołyst [70, 71, 72, 73]. They found that the wall induces parallel alignment and that the nematic phase wets the wall at IN coexistence. For spherocylinders of finite length Dijkstra, Roij and Evans performed computer simulations [74] and calculations within the Zwanzig model [75]. They observed that an isotropic fluid brought in contact with a wall forms a uniaxial surface phase at low densities. At increasing density it undergoes a transition to a biaxial surface phase and finally, when the system approaches the IN transition the wall is completely wet by a nematic film. We will refer to their work in more detail in section 3.2.

Groh and Dietrich studied the isotropic fluid of hard rods close to several curved wall geometries within the Onsager second virial approximation [40]. In particular, they found that the parallel alignment favoured by the surface is stronger if the wall curves towards the fluid than if it curves away from it. In section 3.2 we compare these findings to our simulation results.

3.1 Simulation details

In this part of the work we investigate two different types of systems: in the first case the spherocylinders are confined to a spherical cavity of radius R, in the second case the spherocylinders are are situated outside of the sphere. The second case is achieved by placing the particles in the box with periodic boundary conditions with a big

hard sphere in the center of it. The interaction between a particle and the wall in both cases is hard:

$$U_{\mathrm{r_i}} = \begin{cases} \infty, & \text{if the rod } i \text{ and the wall overlap} \\ 0, & \text{otherwise.} \end{cases} \tag{3.1}$$

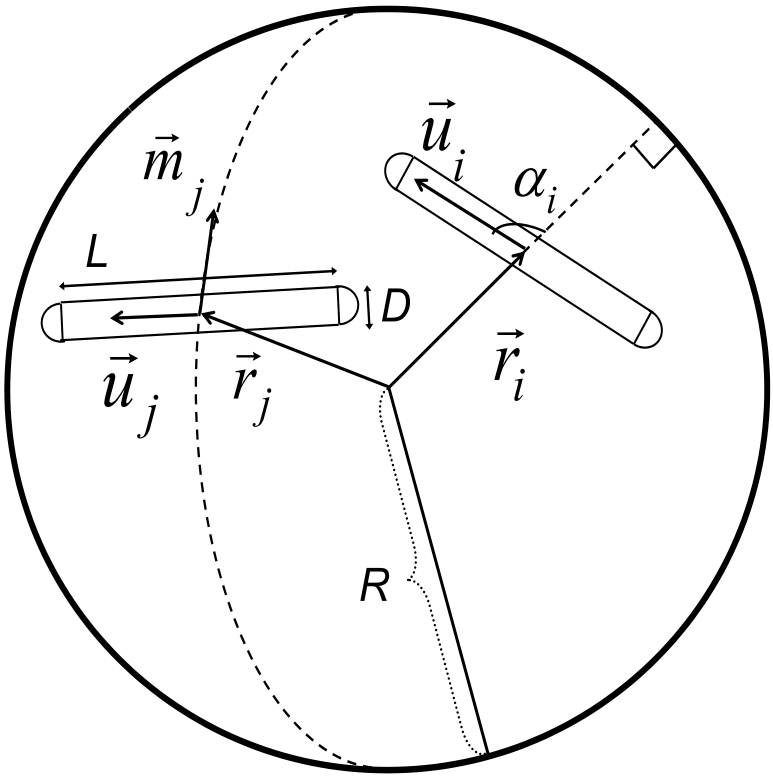

Figure 3.1: Sketch to introduce definitions: The particles are confined into a spherical cavity of radius R. Each particle is a spherocylinder of length L and diameter D. The location of the i-th spherocylinder is given by its centre of mass vector $\vec{r}_i$ and the orientational unit vector $\vec{u}_i$. $\vec{m}_i$ is the local meridian that lies on the plane defined by the z-axis and the radial vector $\vec{r}_i$ of the particle. α is the angle between the orientational vector of the particle $\vec{u}_i$ and the normal to the surface $\vec{n}_i$ drawn from the centre of the particle.

One can point out the advantages of investigating such a system:

i) In the case of a cavity there is no interaction of the droplet with itself due to the periodic boundary conditions;

ii) One does not need additional particles for forming an interface (which is present in case of real droplets in an isotropic media), thus such a system is simpler for computer simulations);

iii) This is a simple way to bend the liquid crystal, which allows to investigate elasticity versus surface anchoring.

We denote the density as the dimensionless quantity $\rho = (L + D)^2 D\, N/V$, where N is the number of particles and V is the volume of the system. The density in the middle of the box is denoted as ρ_{b} for the case of the cavity, for the case of rods outside of a sphere this parameter is defined as their density at the boundary of the box. As a reference we often use the coexistence bulk densities, obtained in [74] by the Gibbs ensemble simulations [76]. The numerical values are $\rho_{\mathrm{i}} = 3.675$ (the density of the isotropic phase) and $\rho_{\mathrm{n}} = 4.300$ (the density of the nematic phase).

Geometry of the system

In the case when the liquid of spherocylinders is surrounded by a curved wall each spherocylinder can approach it only up to a certain distance. This distance is determined by the relative size of the objects (see Figure 3.2) and can be calculated using simple geometrical ideas:

$$\delta = R - \sqrt{(R - 1/2)^2 - (L/2)^2}. \tag{3.2}$$

In this calculation we have used the fact that the distance between the center of mass of the spherocylinder and the wall is minimal when both of its ends touch the wall. This also means that at this position of the particle only one orientation is possible. When the center of mass is situated more than $(L + D)/2$ away from the wall all orientations of the spherocylinder become possible. In the intermediate region the

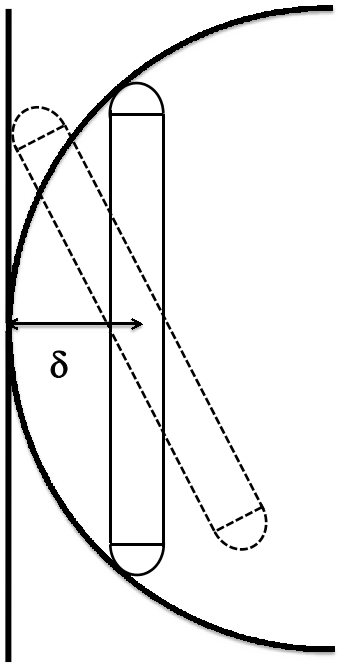

Figure 3.2: A sketch of spherocylinders near a curved wall and a flat one: the "dashed" spherocylinder is allowed near the flat wall and is forbidden near the curved one. We define δ as the width of the "forbidden" layer near the curved wall.

particle gets more possible orientations when it moves further away from the wall.

In order to make sure that a given particle has no overlap with the wall in such a system it is enough to check that both its ends are situated further from the wall than $D/2$.

In the case when the liquid of spherocylinders is situated outside of the sphere the center of mass of a spherocylinder can approach the wall up to $D/2$ (see Figure 3.3). In this case it is more difficult to check if there is an intersection between a particle and the wall or not, because it is not enough to check that both its ends are situated outside of the sphere. The easiest algorithm for doing this is to treat a spherocylinder as a segment P_1P_2, where $P_1 = (x_1, y_1, z_1)$ and $P_2 = (x_2, y_2, z_2)$:

1. Check the ends of the spherocylinder: if both $\sqrt{(x_1^2 + y_1^2 + z_1^2)}$

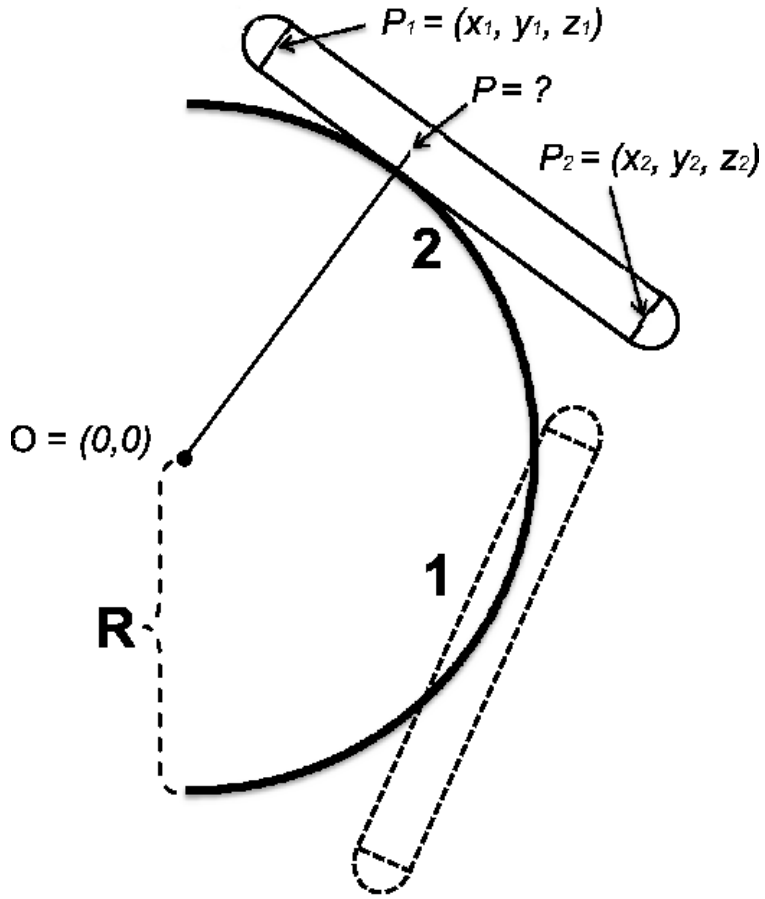

Figure 3.3: A sketch of spherocylinders outside of a hard sphere of the radius R.

and $\sqrt{(x_2^2 + y_2^2 + z_2^2)}$ are larger than $(R + D/2)$ go to step 2. This means that there is no intersection between the ends of the spherocylinder and the sphere, but there is still possibility that the points between P_1 and P_2 can be inside the sphere (like in case of the spherocylinder 2 in Figure 3.2 (b)).

2. Check if the closest to $O = (0, 0, 0)$ point of the line, which the segment belongs to, is situated on the segment. In order to do that one has to use the fact that the closest point on the line P_1P_2 to O belongs to a perpendicular from O to the line. In other words if P is the closest point on the line then

$$(O - P) \cdot (P_2 - P_1) = 0 \tag{3.3}$$

At the same time one can define the points on the line P_1P_2 by a set of equations:

$$P = P_1 + u(P_2 - P_1),$$

or in each coordinate

$$\begin{aligned} x &= x_1 + u(x_2 - x_1), \\ y &= y_1 + u(y_2 - y_1), \\ z &= z_1 + u(z_2 - z_1). \end{aligned} \tag{3.4}$$

After substituting 3.4 in 3.3 and solving the obtained equation for the parameter u one gets

$$u = \frac{(x_0 - x_1)(x_2 - x_1) + (y_0 - y_1)(y_2 - y_1) + (z_0 - z_1)(z_2 - z_1)}{(x_2 - x_1)^2 + (y_2 - y_1)^2 + (z_2 - z_1)^2} =$$

$$= \frac{-x_1(x_2 - x_1) - y_1(y_2 - y_1) - z_1(z_2 - z_1)}{L^2}.$$

If u is not between 0 and 1 then the closest point is not between P_1 and P_2, i.e., the spherocylinder does not intersect the sphere. If it is not so go to step 3.

3. If the closest to O point of the line belongs to the segment P_1P_2 one has to find the distance between this point and O from 3.4: $OP = \sqrt{(x - x_0)^2 + (y - y_0)^2 + (z - z_0)^2} = \sqrt{x^2 + y^2 + z^2}$. If $OP > R + D/2$ there is no overlap between the spherocylinder and the sphere, in other case there is one.

3.2 Isotropic phase

Surface effects in liquid crystals are mainly studied in nematic liquid crystals. The first reason for this is the simplicity of their structure - the local order of aligned molecules can extend to a macroscopic scale. The second reason is that nematic liquid crystals are used in liquid

crystal displays and the surface properties of the display cells play an essential role in their working process.

In this part of the work we focus on the orientational and positional order of an isotropic fluid of spherocylinders near curved hard walls. We only take into account steric interactions between the rods.

Simulation and results

We performed Monte Carlo simulations in the NVT-ensemble. The system was equilibrated by means of local translational and rotational moves. As a first step, we considered spherocylinders of $L/D = 15$ confined to spherical cavities of radii R from 2 L to 10 L. The number of particles was chosen such that we obtained an isotropic fluid in the centre of the cavity. As a reference density we took the density of the isotropic phase at coexistence with the nematic phase in the bulk [74] $\rho_{\mathrm{iso}} = 3.675$. The condition $\rho_{\mathrm{b}} < 3.675$ corresponded to 400-50000 particles depending on the size of the simulated system.

Density dependence

As a first step, we consider, how the structure of our system changes, when the density is changed, while keeping the size of the confining sphere invariant ($R/L = 3.03$).

In Figures 3.4 and 3.5 the equatorial profiles ($\sin\varphi = 0$) of the nematic and the biaxial order parameters are shown for different values of the density ρ_{b}. One can see that in the system with the smallest density ($\rho_{\mathrm{b}} = 2.13$, stars) the nematic order parameter λ_{-} is negative close to the wall and is approximately 0 far from it. The biaxial order parameter Δ is close to 0 everywhere. This means that the spherocylinders form an isotropic phase in the centre of the sphere, while close to the wall there is a layer in which one direction is avoided

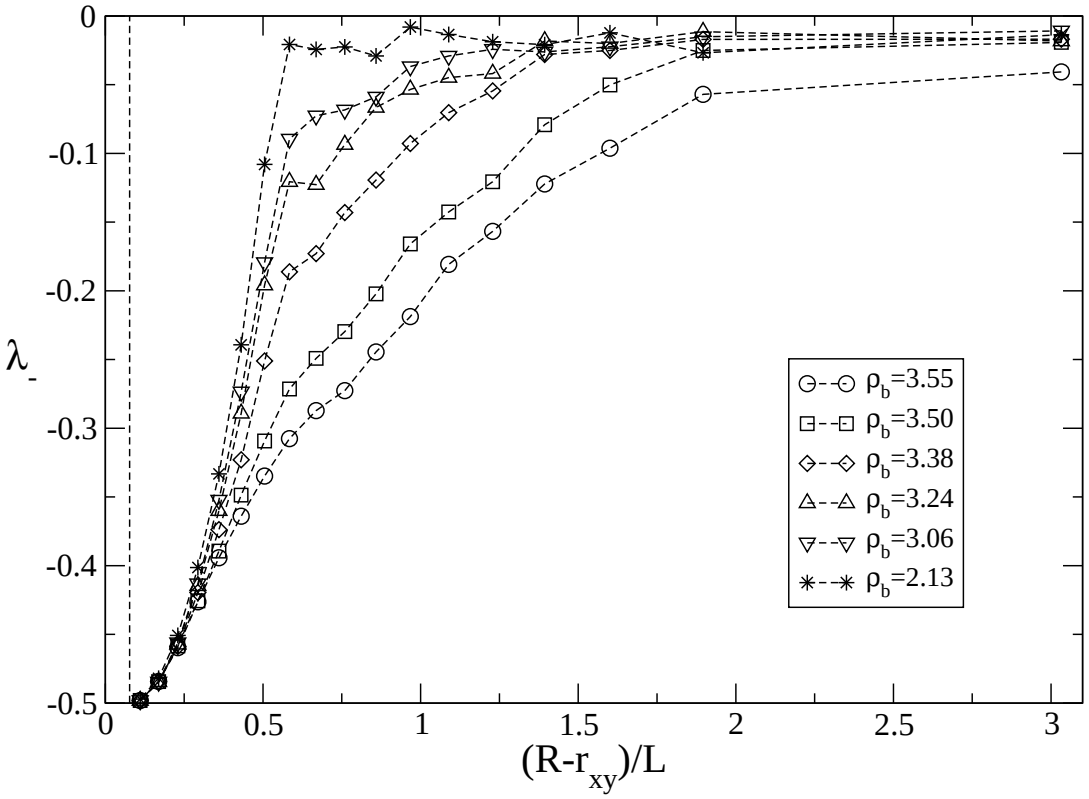

Figure 3.4: Nematic order parameter versus distance from the wall for densities below the isotropic-nematic transition. The vertical dashed line indicates the "forbidden" layer.

(a "uniaxial surface phase"). With increasing density, Δ develops a maximum close to the wall, while it stays 0 in the centre of the sphere. The peak gets wider and higher with increasing density. This indicates that the ordering of the spherocylinders becomes biaxial at the wall at higher densities.

We performed a set of additional runs to estimate the density at which the transition from the uniaxial to the biaxial surface phase occurs. $\Delta(r_{xy} = R)$ increases smoothly with density ρ_b (see Figure 3.6). The transition happens at a density lying in the same range as predicted by theory [75] and estimated in a computer simulation for the same fluid of spherocylinders near a flat wall [74]. However, in the cavity the transition becomes rounded because of finite system size.

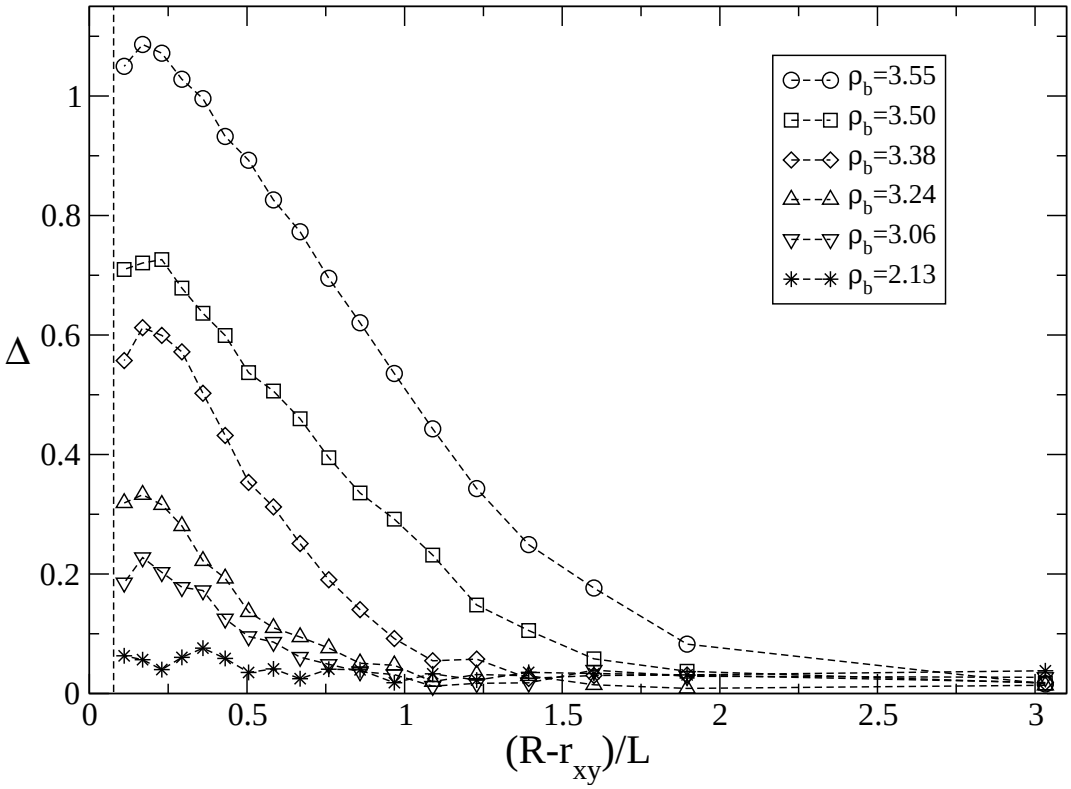

Figure 3.5: Biaxial order parameter $\Delta = \lambda_+ - \lambda_0$ versus distance from the wall for densities below the isotropic nematic transition. The vertical dashed line indicates the "forbidden" layer.

In Figures 3.4 and 3.5 one can see a dashed vertical line at $R - r_{xy} \approx 0.1L$. This line indicates a "forbidden" layer at the curved wall, δ. This "forbidden" layer can be also seen in Figure 3.7 in which the profiles of the local density $\rho(r_{xy}, \sin\varphi = 0)$ are shown for different values of the density ρ_b. All density profiles have a minimum close to the wall at $r_{xy} = R - \delta$. Further from the wall the density increases, reaches its maximum and then levels off into constant value ρ_b. For increasing density the cusp in the density profile moves closer to the wall. This effect can be explained by the profiles of the biaxial order parameter in Figure 3.5, from which we can see that the value of Δ near the wall is increasing with increasing ρ_b, corresponding to a stronger biaxial ordering.

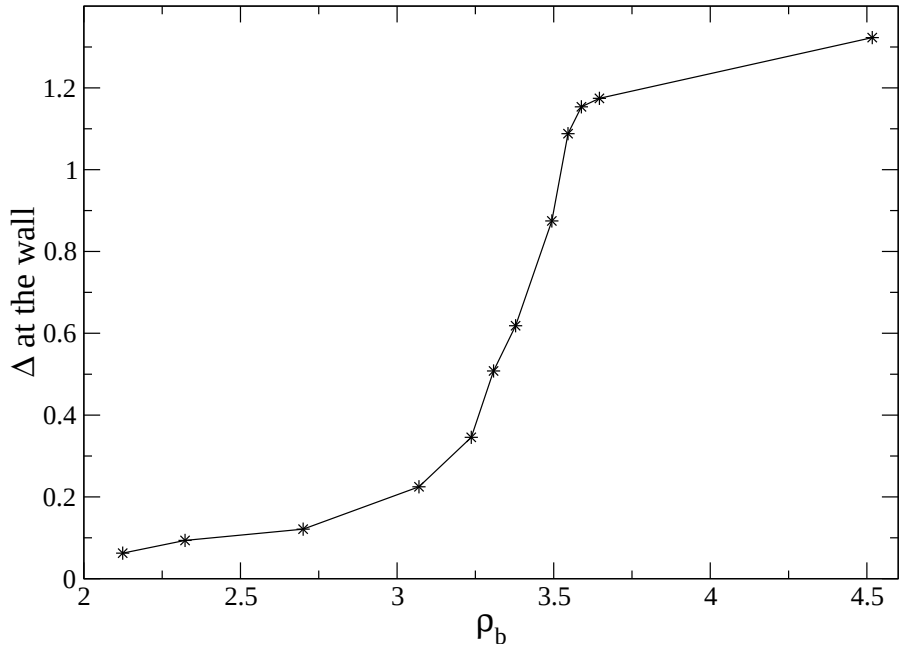

Figure 3.6: Biaxiality at the wall versus density in the centre of the cavity. There is a smooth transition from a uniaxial to a biaxial surface phase at $3 \leq \rho_{\mathrm{b}} \leq 3.5$.

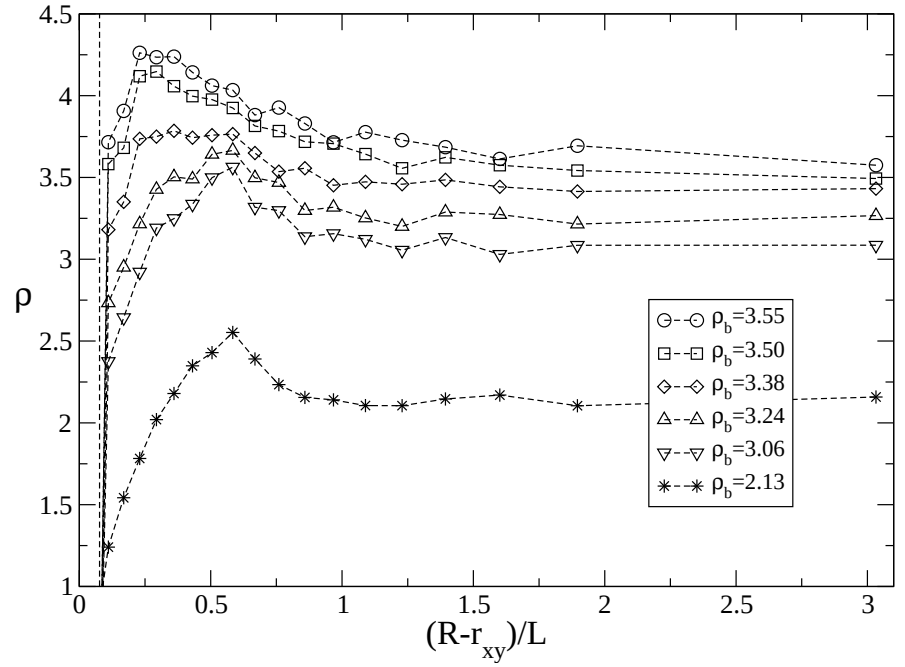

Figure 3.7: Density versus distance from the wall for densities below the isotropic nematic transition. The vertical dashed line indicates the "forbidden" layer.

In Figures 3.4 and 3.5 for small densities λ_- decays rapidly near the wall and slowly further from it. Two length-scales seem to be involved. One is given by correlations with the wall orientation, the other by correlations between the particles.

Figure 3.8 shows the width of the oriented layer (measured as the width of the "inverted peaks" in λ_- at 1/2 of their depth) with respect to the reduced density $(\rho_\mathrm{i} - \rho_\mathrm{b})/\rho_\mathrm{i}$. The width of the layer increases roughly logarithmically as ρ_b approaches ρ_i. However, at the highest examined densities the behaviour changes, because, as one can see from Figure 3.4, for these systems the fluid in the centre of the sphere is not isotropic but has some preferred orientation of the rods. This means that the biaxial layer expands to the whole cavity.

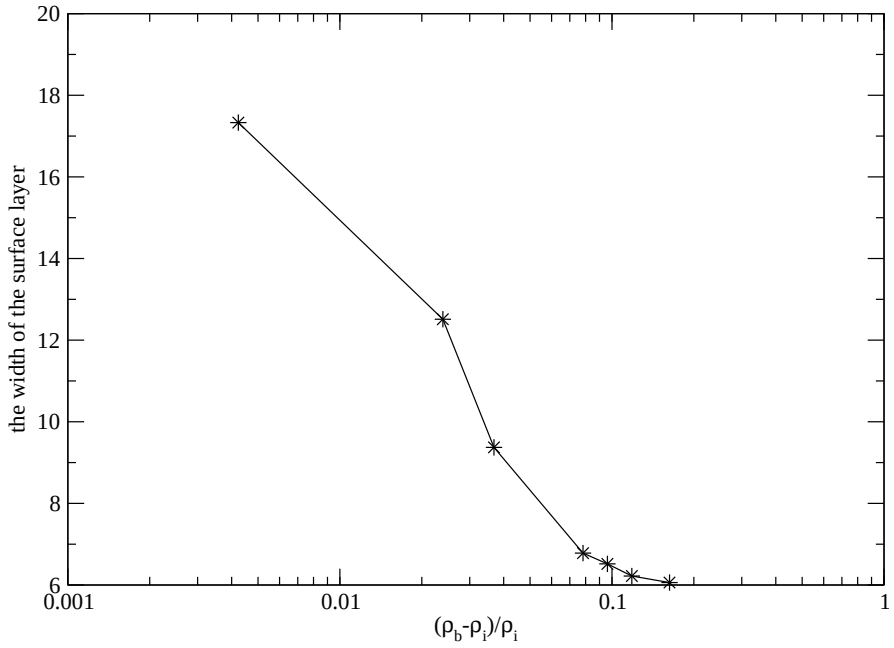

Figure 3.8: Width of the surface layer in the profiles of λ_- versus reduced density $(\rho_\mathrm{i} - \rho_\mathrm{b})/\rho_\mathrm{i}$.

The ordering induced by the wall does not only show up in the orientational order, but also in the adsorption

$$\Gamma = \int \left(\rho\left(r_{xy}, \sin\phi = 0\right) - \rho_{\mathrm{b}}\right) r_{xy}^2 dr_{xy}. \tag{3.5}$$

In Figure 3.9 adsorption Γ is shown versus $\ln\left(\rho_{\mathrm{i}} - \rho_{\mathrm{b}}\right)/\rho_{\mathrm{i}}$. For $0.01 < \left(\rho_{\mathrm{i}} - \rho_{\mathrm{b}}\right)/\rho_{\mathrm{i}} < 0.11$ the adsorption Γ depends logarithmically on $\left(\rho_{\mathrm{i}} - \rho_{\mathrm{b}}\right)/\rho_{\mathrm{i}}$. For values closer to the bulk phase transition the system becomes nematic. Hence the adsorption deviates from the logarithmic behaviour. We fit $\Gamma = a_0 + a_1 \ln\left(\left(\rho_{\mathrm{i}} - \rho_{\mathrm{b}}\right)/\rho_{\mathrm{i}}\right)$ and find $a_0 = -0.31$ and $a_1 = -0.16$. Comparing to the values which were obtained for the Zwanzig model [75] ($a_1 = -0.235$) and in the computer simulation of the same objects near a flat wall [74] ($a_1 = -0.914$), we conclude that in the case of a curved wall the adsorption, i.e. density, grows less.

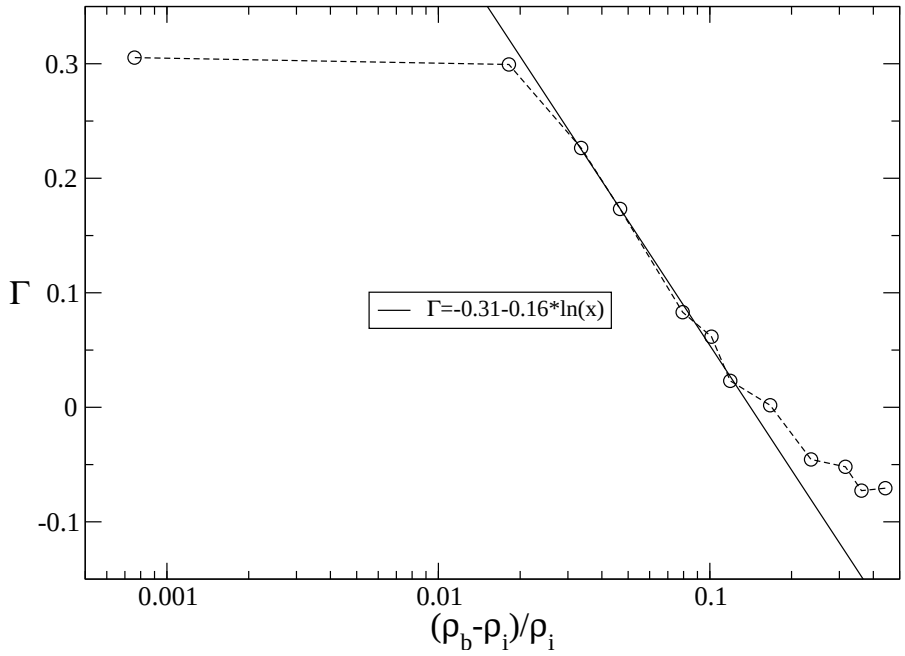

Figure 3.9: Adsorption Γ versus $\left(\rho_{\mathrm{i}} - \rho_{\mathrm{b}}\right)/\rho_{\mathrm{i}}$. For $0.01 < \left(\rho_{\mathrm{i}} - \rho_{\mathrm{b}}\right)/\rho_{\mathrm{i}} < 0.11$ the adsorption depends logarithmically on $\left(\rho_{\mathrm{i}} - \rho_{\mathrm{b}}\right)/\rho_{\mathrm{i}}$. For values closer to the bulk phase transition, the system becomes nematic. Hence the adsorption deviates from the logarithmic behaviour. Fitting $\Gamma = a_0 + a_1 \ln\left(\left(\rho_{\mathrm{i}} - \rho_{\mathrm{b}}\right)/\rho_{\mathrm{i}}\right)$ we find $a_0 = -0.31$ and $a_1 = -0.16$.

Additionally, we present in Appendix A the dependence of the adsorption Γ on $\ln(\rho_{\rm i} - \rho_{\rm b})/\rho_{\rm i}$ for a system of rods confined to a cavity of $R/L = 2$.

Angular distributions

Another interesting question is how the orientations of the rods are distributed in the low-density regime. Let us consider the case $\rho_{\rm b} = 0.95$.

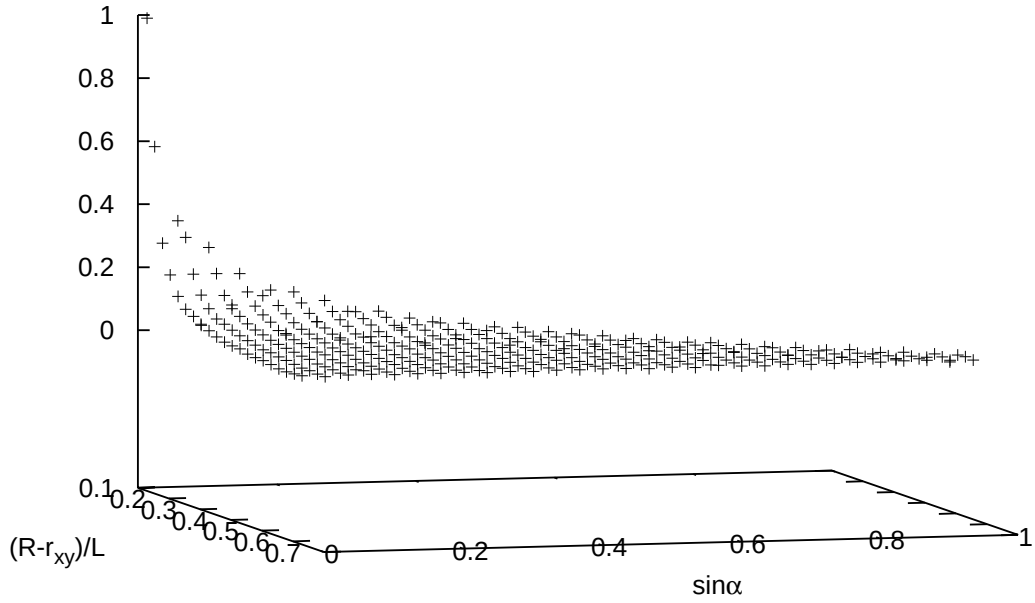

Figure 3.10: Distribution of particles as a function of the rod orientation with respect to the wall plotted for different distances from the wall. The presented data corresponds to the system confined into a spherical cavity with $R = 2.5\ L$, the density of rods in the center of the cavity is $\rho_{\rm b} = 0.95$. At small distances from the wall large values of $\sin\alpha$ are forbidden due to overlap with the wall. Further from the wall one sees equal probabilities to find rods with different $\sin\alpha$.

A typical distribution of particles in a spherical cavity as a function of the rod orientation with respect to the normal to the wall ($\sin\alpha$) is plotted for different distances from the wall ($(R - r_{xy})/L$) in Figure 3.10. At $(R - r_{xy}) < \delta$ none of the orientations are possible. At $(R - r_{xy}) = \delta$ only one rod orientation is allowed ($\sin\alpha = 0$), because

other orientations lead to an overlap with the wall. More orientations become allowed while moving further from the wall, until one moves away to $(L + D)/2$, where rods can not reach the wall directly, and all the orientations become allowed. One can also see that the rod distribution as a function of $\sin\alpha$ is flat at all distances from the wall. This means that the interparticle interactions are negligible.

Curvature dependence

Another way to describe orientational ordering with respect to the surface can be done by introducing the parameter S_{surf}. (Note that the pre-factor differs from the definitions of S_{bip} and S_{z} in order to facilitate comparison with the work by Groh and Dietrich [40])

$$\begin{aligned} S_{\mathrm{surf}}(r_{xy}) &= \langle 1/N(r_{xy}) \sum_{i=1}^{N(r_{xy})} \sqrt{5/(4\pi)} P_2(\vec{u}_i \cdot \vec{n}_i) \rangle = \\ &= \langle 1/N(r_{xy}) \sum_{i=1}^{N(r_{xy})} \sqrt{5/(16\pi)} (3\cos^2\alpha_i - 1) \rangle, \end{aligned} \tag{3.6}$$

where α is the angle between the orientational vector of the particle $\vec{u}_i$ and the normal to the surface $\vec{n}_i$, drawn from the centre of the particle (Figure 3.1).

We show the profiles of this parameter in Figure 3.11 for systems of $\rho_{\mathrm{b}} = 0.95$ and various radii. Close to the wall only the alignment parallel to the wall is allowed ($\alpha = \pi/2$), from this follows that $S_{\mathrm{surf}}(r_{xy} \to 0) = -\sqrt{5/(16\pi)} = -0.3154$. We can see this in the profiles for $r_{xy} \to (R - \delta)$. In the case of a random distribution one would get $S^{\mathrm{iso}}_{\mathrm{surf}} = 0$. Negative values of S_{surf} indicate a preference of particles to lie parallel to the wall. S_{surf} is negative for distances from the wall that are less than $(L + D)/2$, and 0 further away. The alignment is stronger in the case of more strongly curved walls. This is explained by the fact that the curved wall restricts the possible orientations of the particles more strongly (see Figure 3.2).

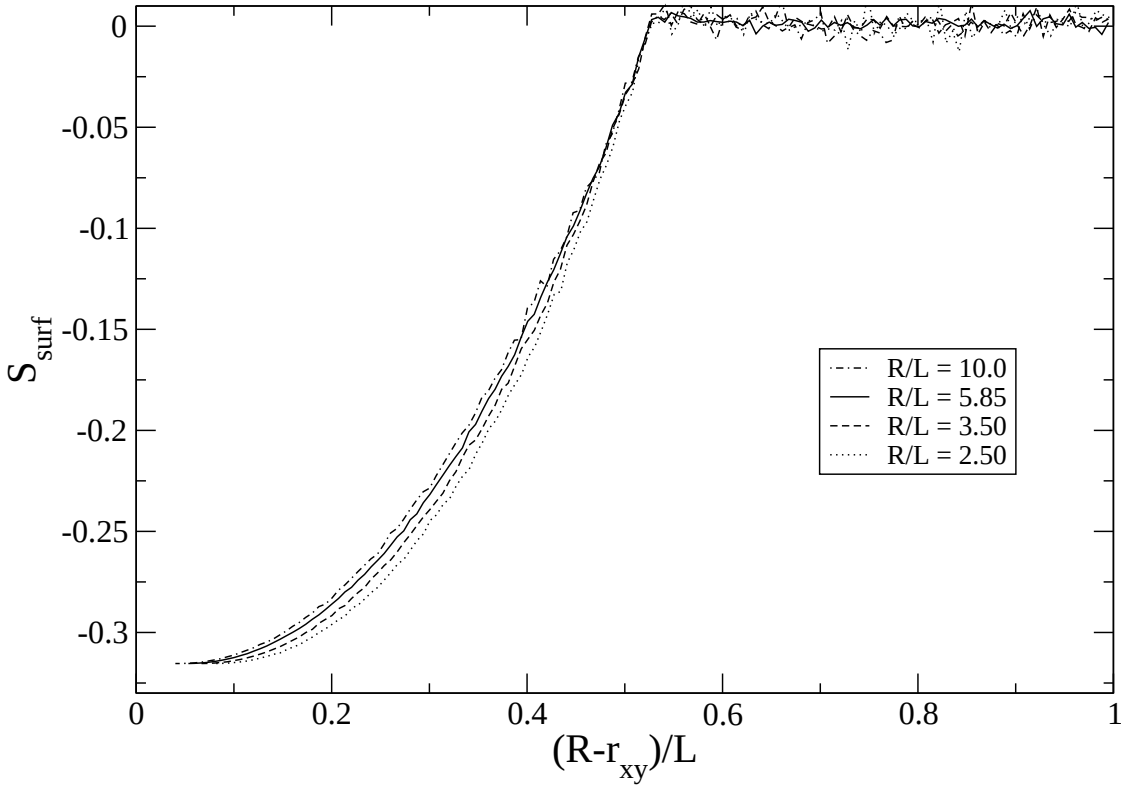

Figure 3.11: Order parameter S_{surf} at a fixed density $\rho_{\mathrm{b}} = 0.95$ for different wall curvatures. Parallel orientations to the wall, i. e., negative values of S_{surf} are more favoured by strongly curved walls.

Outside of the sphere

As a next step, we consider a system of spherocylinders in a cubic box with a side length $13.\bar{3}\ L$, applying periodic boundary conditions. We put a hard sphere of $R = 2.5\ L$ in the center of this box, thus, making it forbidden for the spherocylinders to enter this volume. This implies that we observe a liquid of rods near a wall, which curves away from the liquid. The number of rods was chosen such that $\rho_{\mathrm{b}} = 0.95$.

After equilibrating the system, we obtain the distribution of particles as a function of the distance from the wall and orientation with respect to it which looks essentially the same as in Figure 3.10, however in this case there is no forbidden layer at the wall, because of the

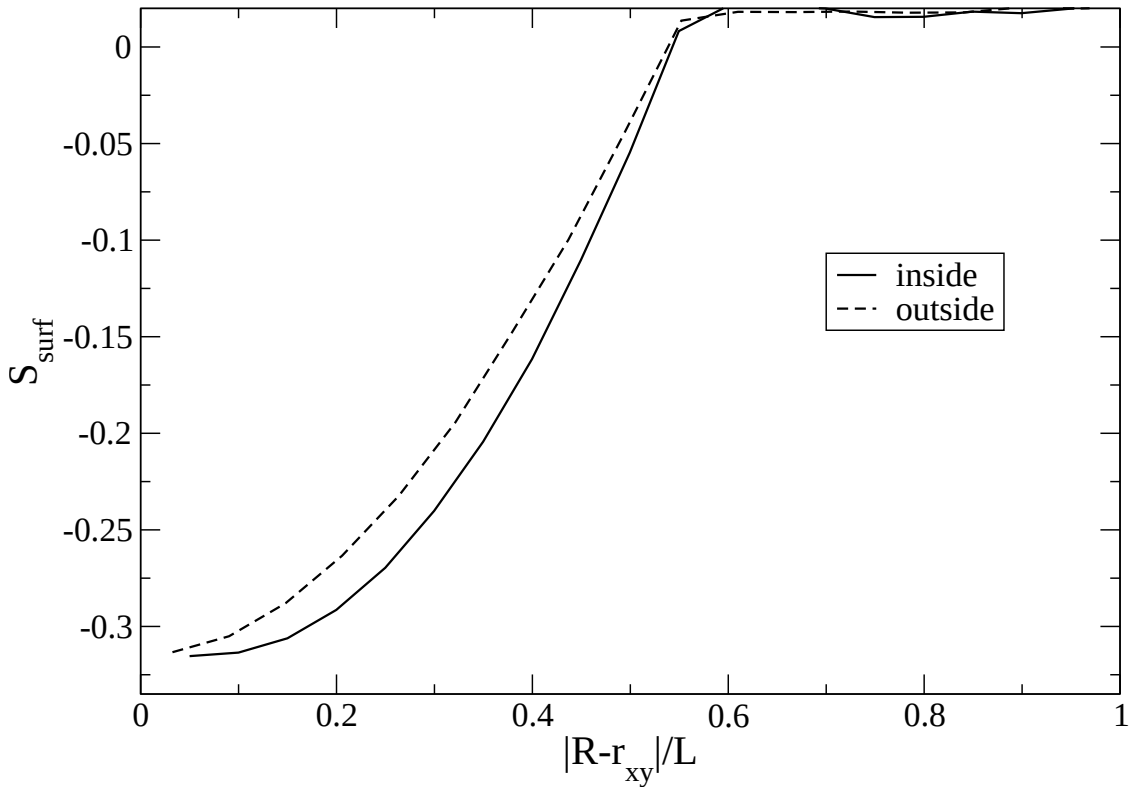

Figure 3.12: Order parameter S_{surf} as a function of the distance from the wall for the system outside of the hard sphere with $R = 2.5\ L$ in comparison with an analogous profile for a system inside a cavity with $R = 10\ L$ (a solid line). The wall, that is curved away from the fluid, makes parallel orientations to the wall, i. e., negative values of S_{surf} less favourable than in the case if a wall is curved to the fluid.

different geometry.

In Figure 3.12 we present the dependence of S_{surf} on the distance from the wall for the two systems: spherocylinders outside of a sphere ($R = 2.5\ L$) and inside a cavity ($R = 10\ L$). It is obvious that in the first case $|S_{\text{surf}}|$ near the wall is smaller than in the second case. One can conclude that curving the wall away from the fluid makes orientational ordering less favourable than in the case of curving it in the direction to the fluid.

It would be interesting to obtain the dependence of adsorption on the density of the rods in a system with such a curvature. However,

this investigation turned out to be too time consuming because the growth of the layer at the wall occurs at the densities, approaching the isotropic-nematic transition. This in turn implies a big amount of particles (this amount is much larger than in the case of the cavity geometry because one has to take the box large enough to minimize the finite size effects).

Conclusions

We have studied a fluid of hard spherocylinders with $L/D = 15$ confined to a spherical cavity of $R/L = 2.5 \ldots 10$. We have performed simulations for different values of the system density. At low values of the density we have observed an isotropic phase in the middle of the cavity and a layer of particles lying parallel to the wall at the surface. The curved wall favours parallel alignment. When the density of the system is increased the oriented layer grows. As predicted by Groh and Dietrich [40] a curved wall produces stronger parallel anchoring than a flat wall. This result was compared to the case of the same fluid of spherocylinders located outside of a hard sphere of $R/L = 2.5$ and it was found that in the latter case the orientational ordering is less favoured.

Also at low densities we have observed a rounded surface transition in a cavity from a uniaxial to a biaxial phase.The thickness of the biaxial (nematic) layer at the surface increases logarithmically with the density until the entire cavity is filled with a nematic phase.

We also computed the adsorption at the wall. While orientational ordering is favoured by the curved wall, adsorption is disfavoured, compared to the case of a flat wall.

Summarizing, the wall curved to the fluid induces an ordered layer. At low densities this layer is uniaxial, at higher densities it is biaxial (as it is in the case of a flat wall). Compared to the flat wall, however,

orientational ordering is stronger, while adsorption is weaker. Hence the two main properties of the system which jump at the isotropic nematic transition, density and orientational order, are influenced in opposite ways by a curved wall. The case of the wall curved away from the fluid needs further investigations.

3.3 Nematic phase

In this part of the work we focus on the orientational order of a nematic liquid of spherocylinders confined into a spherical cavity.

Simulation and results

As before, we performed Monte Carlo simulations in the NVT-ensemble, and equilibrated the system by means of local translational and rotational moves. We considered spherocylinders of $L/D = 15$ confined to spherical cavities of radii R equal to 2 L, 2.5 L and 3.03 L.

Now we consider densities beyond the isotropic nematic transition. In order to describe the orientational order in the nematic phase we calculate the bipolar order parameter S_{bip} which is defined as

$$S_{\text{bip}}(r_{xy}, \varphi) = \langle 1/N(r_{xy}, \varphi) \sum_{i=1}^{N(r_{xy},\varphi)} P_2(\vec{u}_i \cdot \vec{m}_i) \rangle, \tag{3.7}$$

where P_2 is the second rank Legendre polynomial, $\vec{u}_i$ is the orientation vector of particle i and $\vec{m}_i$ is the local meridian that lies on the plane defined by the z-axis and the radial vector $\vec{r}_i$ of the particle (Figure 3.1).

The alignment with respect to the z-axis is characterized by

$$S_{\text{z}}(r_{xy}, \varphi) = \langle 1/N(r_{xy}, \varphi) \sum_{i=1}^{N(r_{xy},\varphi)} P_2(\vec{u}_i \cdot \vec{e}_z) \rangle, \tag{3.8}$$

where $\vec{e}_z$ is the unit vector pointing in the z direction.

S_{bip} and S_z are shown in Figures 3.13 and 3.14 for a system with $R/L = 3.03$ and $\rho_{\text{b}} = 4.55$. The density of the nematic phase at coexistence with the isotropic phase in the bulk [74] is $\rho_{\text{nem}} = 4.3$. The S_{bip} parameter shows how close the configurations are to a bipolar one. The lines in Figure 3.13 point in the direction of a perfectly bipolar field and their lengths correspond to the strength of alignment. Some small deviations can be seen at the poles of the sphere, while most of the field is bipolar. The S_z parameter measures the alignment of the director field with a homogeneous field. There are clear deviations. These findings are in agreement with the observations of Zannoni and co-workers [61, 62].

We have varied the size of the system and its density and in all cases we found only the bipolar structure. Comparing to the arguments by Prinsen and van der Schoot [56] this implies that the energetic contribution from elastic deformations of the nematic director field is smaller than the contribution of the surface anchoring energy for all the examined system sizes and densities.

However, the structure, which we obtain, differs from the ideal bipolar one (see Figure 3.13). This gives rise to the question: what properties does the defect on the poles have?

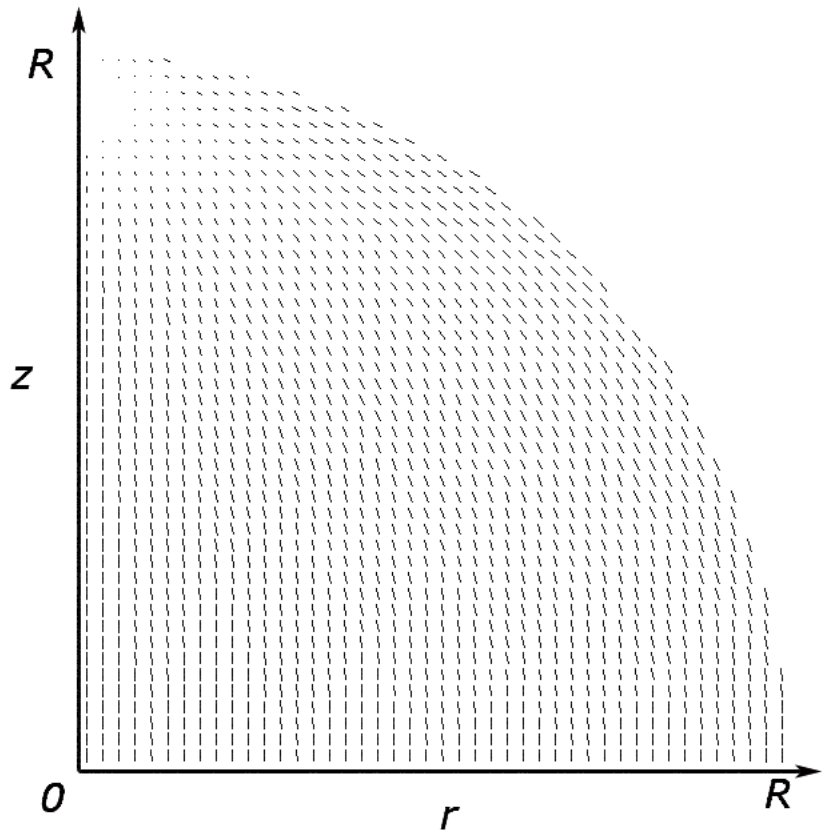

Figure 3.13: Alignment with respect to an ideal bipolar structure: the lines point in the direction of the meridians, their length is given by the bipolar order parameter S_{bip}.

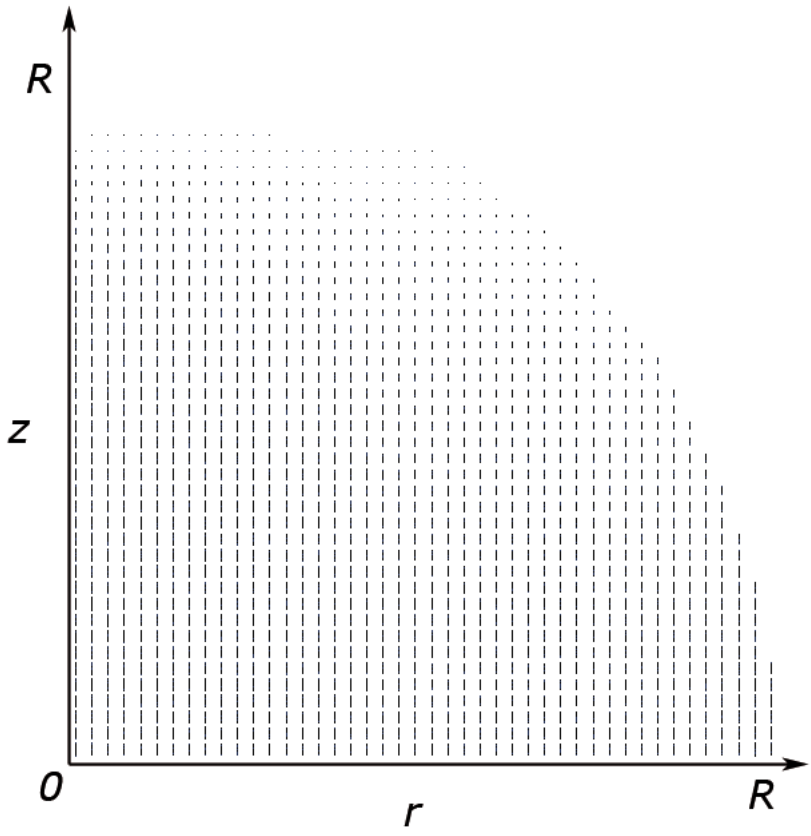

Figure 3.14: Alignment with respect to an ideal homogeneous structure: the lines point in the z-direction, their length is given by the order parameter S_z.

Defects on the poles of the sphere

Figure 3.15 shows the dependences of the eigenvalues of the orientational tensor $\mathbf{Q}$ of the particles lying on the z-axis of the system (which is defined as the orientation of the overall nematic director field) on the distance from the pole of the sphere ($R/L = 3.03$, $\rho_{\mathrm{b}} = 4.55$). From the graph one can conclude that there is a highly ordered nematic phase in the centre of the sphere. At a distance from the wall $z \sim L$ the nematic order parameter starts decaying until it reaches its minimum at $z \sim L/2$. At the same time one can see that at $z \sim L/2$ the difference between λ_- and λ_0 starts growing, indicating a presence of a biaxial structure. Directly at the wall ($z = 0$) $\lambda_+ = \lambda_0$, while $\lambda_- = -0.3$, this means the system forms an uniaxial surface phase at the wall. At this point one has to take into account that the averaging was done assuming the radial symmetry.

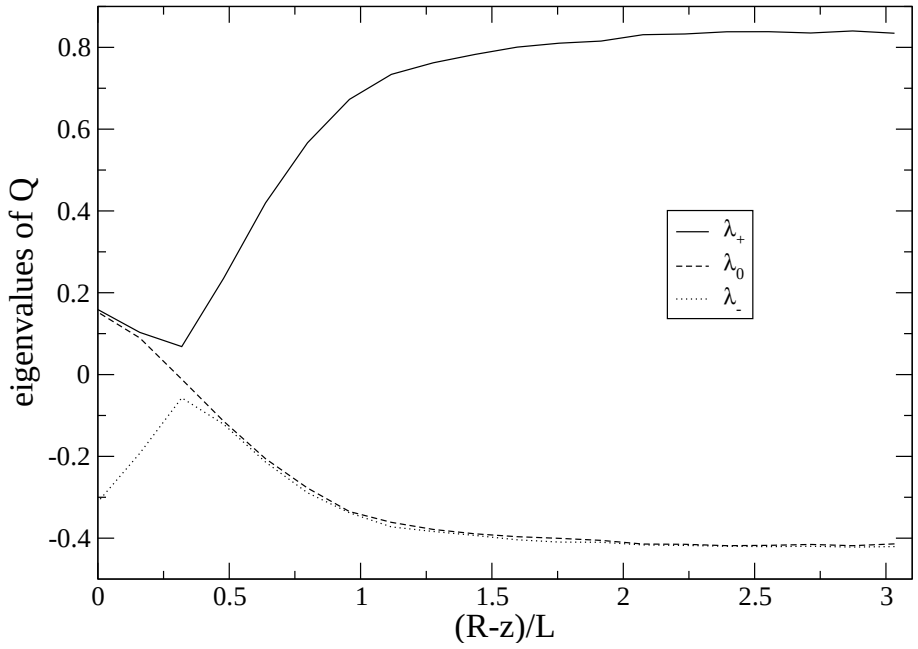

Figure 3.15: Eigenvalues of the orientational tensor $\mathbf{Q}$ for the particles lying on the z-axis of the system versus the distance from the pole of the sphere. The defect extends roughly $L/2$ into the sphere.

We observe similar behaviour in systems with different values of the radius R of the confining sphere (see Appendix B). One can notice that for $R/L = 2$ the defect is slightly thinner, however, the obtained data is not sufficient for making any stronger conclusion.

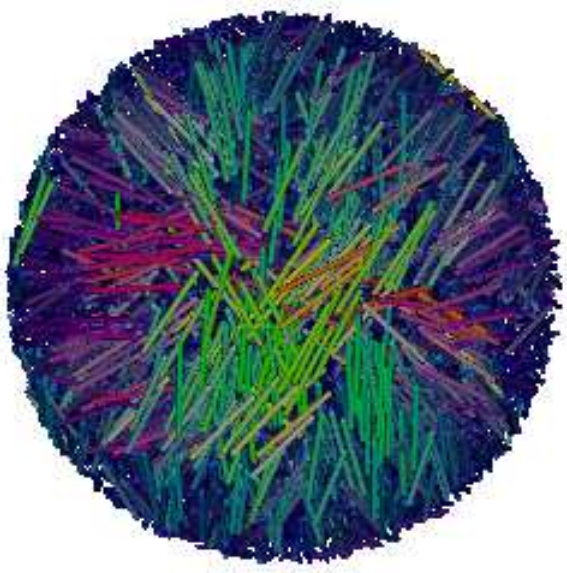

Figure 3.16: A typical snapshot of a pole of the sphere. The particles are colour-coded according to their orientations.

To get a better understanding of the structure of the defect we inspect snapshots of the system. A typical one is presented in Figure 3.16, in which the droplet is seen "from the top" i.e. looking at one of the poles. We never observe an ideal "bipolar" configuration, which means that a boojum defect is energetically too expensive. Using this fact and taking into account the analysis of the values of the eigenvalues of the orientational tensor we conclude that the point defect splits into a line of strength $k = 1/2$ defects which extends roughly to $r = L/2$ into the droplet.

We could not investigate this in more detail because the averaging procedure needs to project conformations onto each other with respect to the nematic director of the entire droplet and the local director at

the pole. As both quantities are subject to strong fluctuations, the quality of the averaged data is not high enough to allow for further conclusions.

Conclusions

Simulations at higher densities (beyond the bulk nematic coexistence density in the centre of the sphere) always produced bipolar droplets. This is consistent with theoretical predictions [56] if one assumes that for this model the energetic contribution due to the anchoring strength ω is always larger than the energetic contribution due to the elasticity.

The obtained bipolar structure differs from an ideal one in which the particles form boojums at the poles of the sphere. Apparently this type of defect is energetically too expensive. The point defect probably splits into a line of $k = 1/2$ defects which extends roughly to $r = L/2$ into the droplet.

Chapter 4

Suspension of rods and spheres

Hard-rod fluids exhibit a wealth of aggregated states including nematic, smectic and columnar liquid-crystalline phases as well as various plastic and crystalline solid phases, depending on the precise shape, density and composition of the model particles present in the system [14]. Arguably, the experimentally and theoretically by far most extensively studied liquid-crystalline state is the nematic that is characterized by uniaxial and up-down symmetry. The transition from the isotropic to the nematic phase is first order (see, however, the work by Oakes and co-workers [77]), and in the biphasic region it proceeds via the formation of nematic droplets called tactoids in the background isotropic dispersion. Tactoids are typically not spherical but elongated and spindle-shaped, and they have over the past century or so been observed in a wide variety of systems [78, 79, 80, 81, 82, 83]. The shape and internal structure of nematic droplets is the result of the competition between the preferred surface anchoring of the director field, and the deformation of the director field that occurs if the preferred anchoring is indeed accommodated.

The shape and director-field configuration of tactoids have recently been studied theoretically in considerable detail within a macroscopic Frank elasticity theory [56, 57, 58, 84, 82]. Predictions depend on

several parameters: two surface energies (the surface tension and anchoring energy), three bulk elastic constants associated with the splay, twist and bend deformations, the saddle-splay surface elastic constant, and, finally, the size of the droplet. For our purposes, it is enough to summarize the most important predictions, presuming preferential planar anchoring of the director field to the interface that for rod-like particles seems to hold for entropy reasons: i) The director field of small drops is uniform and of large ones bipolar; ii) The crossover is smooth and set by a healing or extrapolation length that is the ratio of an average elastic constant and an anchoring energy; iii) The aspect ratio of uniform tactoids depends only on the anchoring energy, and of bipolar ones on their size relative to the healing length.

Some aspects of these theoretical predictions have been verified against experiment, in particular the size dependence of aspect ratio and opening angle of the sharp ends of the tactoids [84, 82, 57, 58, 81]. The crossover from bipolar to uniform director field has not been observed and this probably presents quite an experimental challenge because it has been predicted to occur when the drops are quite small, that is, in the micrometer range. For such small droplets, not at all very much larger than the particles that they are made up from, director field patterns are difficult to distinguish in polarization microscopic images.

Clearly, computer simulations are of use here [25, 59, 60], not least because a macroscopic description might break down for such small drops, in other words, the predicted transition may be spurious. On the other hand, recent simulations on the nucleation of the nematic phase in a hard-rod fluid have indeed shown that small nuclei of the nematic phase are elongated and it appears at least that their director field is uniform [85]. Simulations on small nematic droplets of prolate particles interacting via a Gay-Berne potential have been shown to exhibit similar behavior, although fluctuations are large so a director

field is not so easily defined [86, 87]. Because systematic computational investigations of the shape and internal structure of nematic droplets are lacking, we set out to do this for nematics of hard spherocylinders of aspect ratio ten and now focus on actual drops that can adjust their structure. This we do using an extension of the Asakura-Oosawa-Vrij or AO model for colloid-polymer mixtures [88, 89] to anisotropic colloids [44]

The Asakura-Oosawa-Vrij model was originally developed as a useful model for mixtures of polymers and spherical colloids. In this model the polymers are modeled as spheres, which are freely interpenetrable with respect to each other, while there is a hard-core repulsion between the colloids as well as between the colloids and the polymer spheres. Then the interaction energy is equal to zero, if there are no forbidden overlaps, or is infinite, if some are present. Thus, the phase behaviour is purely of entropic origin.

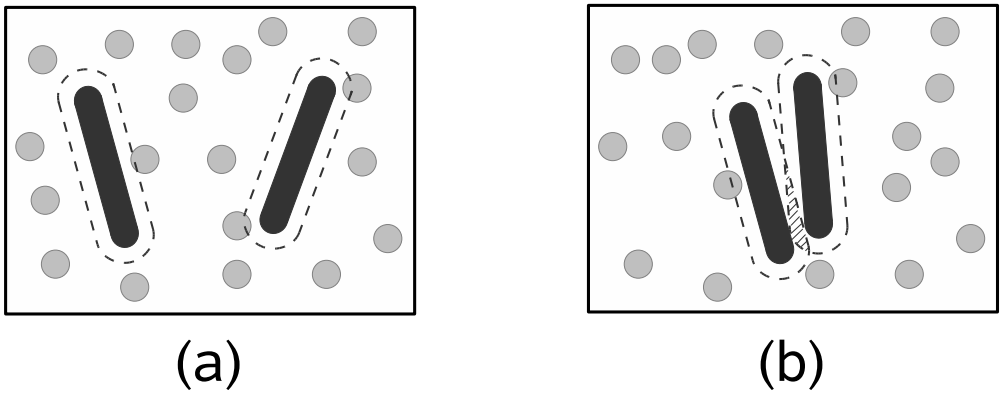

Figure 4.1: A schematic representation of two hard spherocylinders surrounded by a gas of non-interacting spheres. The dashed lines indicate the depletion zones of the spherocylinders. The shaded area is the overlap region between the depletion zones.

It was found that the colloidal particles attract each other via depletion forces, which are indeed entropically induced. For instance, one can consider two of such hard particles in a suspension of spheres,

which may overlap with each other, but not with the colloids (we give a schematic representation of a system with two hard spherocylinders in Figure 4.1). There is a zone around each of the colloids, where the centres of masses of spheres have no access to. This zone is called the "depletion zone" and is indicated by dashed lines in Figure 4.1. If the particles come close to each other, such that these zones can overlap (a shaded area in Figure 4.1(b)), the volume accessible to the spheres becomes larger, thus, increasing their translational entropy. On the other hand, the colloidal particles loose their translational entropy because of coming close to each other. Hence, the strength of the interactions is determined by the concentration and the size ratio. In the case of colloidal rods, which is considered here, the orientational entropy is also important. The more the rods are aligned, the larger the overlap of the depletion zones is, leading to an increase of the entropy of the spheres. However, in the same time, the orientational entropy is decreased due to the fact that rotations of each of the rods are restricted by the presence of the neighbouring one.

In conclusion, the depletion forces in the Asakura-Oosawa-Vrij model are based on an interplay between the translational entropies of colloids and polymers in the case of spherical colloids. In the case of colloidal rods one more contribution to the overall entropy exists, and that is the orientational entropy of the rods.

Mixtures of rod-like particles with depletion interactions attracted some interest in the last years. Theoretical predictions of the phase behaviour for different rod lengths were made by means of the free volume theory [90, 91] . The effect of the addition of depletant on the isotropic-nematic phase transitions in mixtures of the boehmite rods [92] and carbon nanotubes [93] was studied experimentally. A non-adsorbing polymer, dextran, was used to induce a phase separation in aqueous dispersions of filamentous fd virus particles [80]. Also Monte Carlo simulations of rods with depletion interactions, modeled as an

effective potential between the rods, were performed to locate phase boundaries via thermodynamic integration [94, 95].

In this Chapter we use the predictions for the phase diagram of a mixture of spherocylinders of length $L/D = 10$ and spheres in order to investigate systems in which a phase separation occurs, and a nematic droplet in an isotropic medium is formed. This is done in Section 4.1, the relevant model and simulation details are provided in Section 4.1.1, the results of the simulations are discussed in Section 4.1.2.

Further investigations, which are presented in Section 4.2, are based on the method proposed by Grünwald [96, 97]. The idea of this method is to use spheres of larger diameter because this allows to obtain phase separation using a much smaller amount of spheres. This method allows us to compress by osmotic stress droplets of a fixed number of rod-like particles. This is achieved in a controlled manner because the density of the rods in the drop is set by the imposed pressure of the ideal gas of spheres (if we ignore a small contribution from the Laplace pressure). Hence, the drop size is then given by the number of rods in the simulation box. We introduce the model and the simulation details in Section 4.2.1. A detailed discussion of our results is given in section 4.2.2. Finally, in section 4.2.3 we summarize our findings and relate them to theory and experiment.

4.1 Rods and spheres of the same diameter

4.1.1 Model and simulation details

We consider a system of hard spherocylinders (see Chapter 2) with an aspect ratio of $L/D = 10$ suspended in a gas of spheres. The spheres of the same diameter as spherocylinders $D_{\mathrm{sp}} = D$ are hard with respect to the spherocylinders and freely interpenetrable among each other. So, the rod-rod ($\mathrm{r_i r_j}$), rod-sphere ($\mathrm{r_i sp_j}$) and sphere-sphere

($\mathrm{r_i r_j}$) interaction potentials are

$$\begin{aligned} U_{\mathrm{r_i r_j}} &= \begin{cases} \infty, & \text{if rods } i \text{ and } j \text{ overlap} \\ 0, & \text{otherwise} \end{cases} \\ U_{\mathrm{r_i sp_j}} &= \begin{cases} \infty, & \text{if the rod } i \text{ and the sphere } j \text{ overlap} \\ 0, & \text{otherwise} \end{cases} \\ U_{\mathrm{sp_i sp_j}} &= 0. \end{aligned} \tag{4.1}$$

This model is an extension of the Asakura-Oosawa or AO model for colloid-polymer mixtures [88, 89] to anisotropic colloids [44]. Note that strictly speaking in our case the spheres do interact with each other via the rods.

The simulations were performed in the NVT-ensemble in a cubic box of the volume $V = 36^3 D^3$ and $46^3 D^3$ with periodic boundary conditions. The number of spherocylinders in the box was varied from approximately $N_\mathrm{r} = 350$ to $N_\mathrm{r} = 1600$, the number of spheres N_sp was varied from approximately 20000 to 50000.

All the simulations were started from configurations in which all the rods formed a spherical nematic droplet, which was surrounded by a gas of spheres.

The systems were equilibrated by local (translational and rotational) moves of single particles and by cluster moves. The basic idea of the cluster move is to exchange the positions of one spherocylinder and of some spheres. In order to do this, we first choose a random spherocylinder and a random position, in which we will try to insert it. Then we choose a random new orientation. We show schematically an example of a system in Figure 4.2(a), where the spherocylinder is shown in its original position, and the dashed line shows the space which the spherocylinder will occupy in a new position (including the depletion zone). We reject the move if any spherocylinder intersects this volume. Otherwise, if there are intersections only with

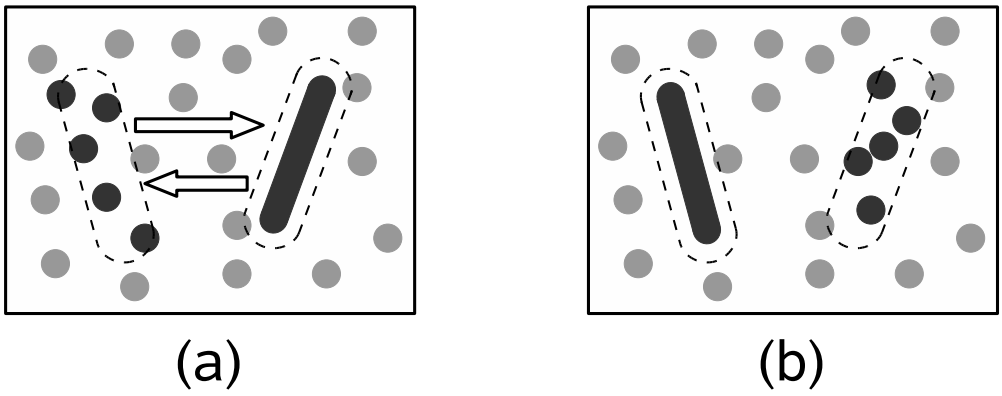

Figure 4.2: A schematic representation of a cluster move in a system of spherocylinders and spheres, the dashed lines indicate the original and the final depletion zones of the chosen spherocylinder, the dark-grey particles have to be moved to a new position: a) the initial configuration; b) the final configuration.

some spheres, we remove them and insert randomly in the space which was originally occupied by the chosen spherocylinder, the latter one being moved to its new location (see Figure 4.2(b)).

4.1.2 Results

In Figure 4.3 we show a phase diagram of the AO-model for a mixture of spherocylinders of length $L/D = 10$ and spheres of the same diameter as spherocylinders, calculated [98] using the free volume theory [91] combined with a numerical minimization technique [99]. The horizontal axis corresponds to the total volume fraction of spherocylinders $\nu_{\rm r} = N_{\rm r} v_{\rm r}/V$, here $v_{\rm r}$ is the volume of a single spherocylinder. The vertical axis corresponds to the total volume fraction of spheres $\nu_{\rm sp} = N_{\rm sp} v_{\rm sp}/V$, here $v_{\rm sp}$ is the volume of a single sphere.

The aim of this work is to investigate nematic droplets suspended in an isotropic medium. We show by different symbols in Figure 4.3 the total volume fractions of spherocylinders and spheres in the systems, which we investigated.

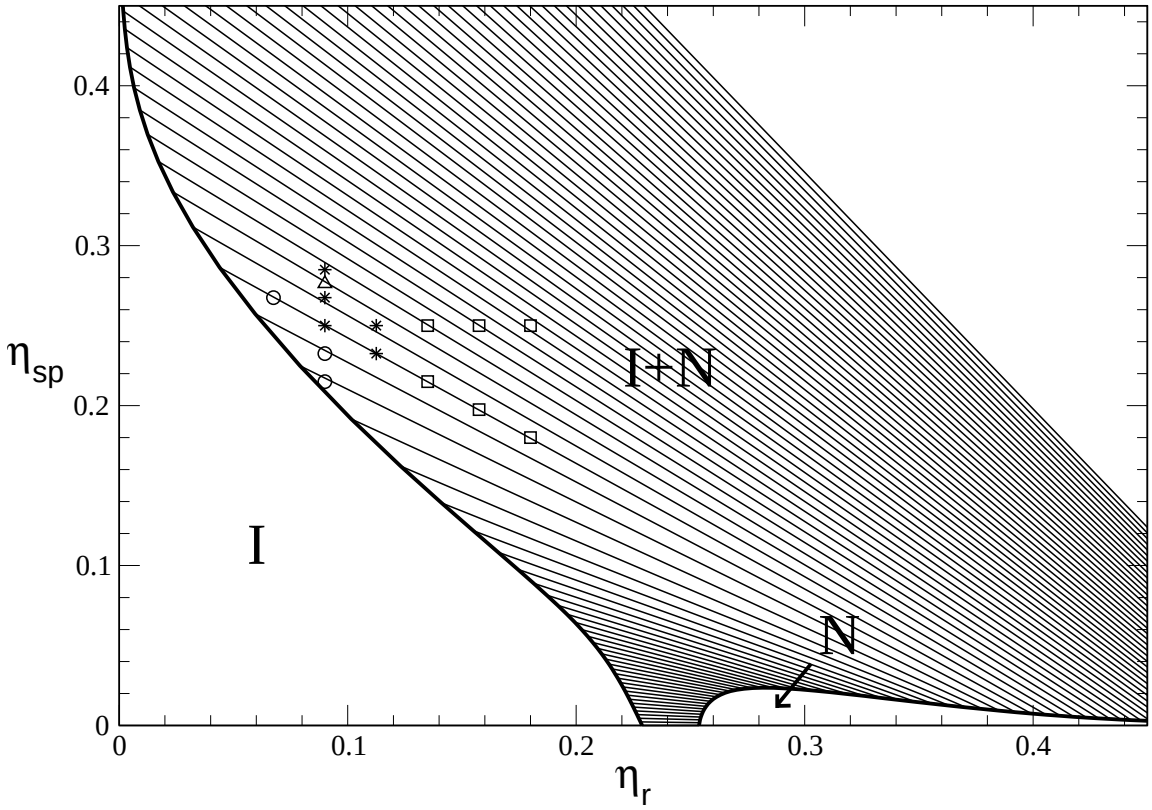

Figure 4.3: Phase diagram for the AO-model of spherocylinders with $L/D = 10$ and spheres with $D_{\rm sp} = D$. The horizontal and vertical axes show the volume fraction of spherocylinders and spheres, respectively. The thick lines are the coexistence lines for the isotropic-nematic transition obtained from free volume theory combined with a numerical minimization technique [98], the thin lines connect the coexistence points on the diagram. I and N refer to isotropic and nematic phases, respectively. The symbols on the diagram indicate the compositions of the systems which were investigated in the current work, different types of them show the result after equilibration: circles are used for mixed systems, the triangle and stars are used for a nematic droplet in coexistence with an isotropic medium, squares are used for either nematic tubes or layers.

These points were chosen in the region of the phase diagram in which a nematic phase coexists with an isotropic phase with a relatively low density of spherocylinders, because an isotropic phase with a high density of spherocylinders implies a considerable increase of their amount for obtaining nematic droplets of the same size, and this is crucial for the simulations, because most of the simulation time is used for checking overlaps between spherocylinders and the neighbouring particles.

In the systems, which are indicated by circles on the diagram 4.3, spherocylinders and spheres became totally mixed after equilibration and form an isotropic phase. However, according to the phase diagram demixing has to occur in these systems. This difference can be explained either by lacking accuracy of the theoretical predictions or by the finite size effects in the simulated systems which can result in the instability of small droplets.

In all other investigated systems, demixing occurs and two phases are formed, sphere-rich and spherocylinder-rich, the first one being isotropic and the latter one nematic. If the surface-to-volume ratio of the spherocylinder-rich phase is large enough one can observe droplets in an isotropic medium. In this case the isotropic medium is a lower density phase containing the same material and so the droplet can exchange material with the surrounding medium. We indicate such systems by stars and a triangle on the diagram. Otherwise, the volume part of the nematic phase is too big and it forms a tube or a layer, such systems we indicate as squares on the diagram.

The droplets, which we obtained in the systems indicated as stars on the phase diagram, can be quite easily visually distinguished from the surrounding medium. However, for computational purposes one has to use some algorithm for defining a cluster. We determine the clusters by the criterion that two spherocylinders i and j belong to the same cluster if (i) their surface-to-surface distance is not larger than

0.5 D and (ii) $|\vec{u_i} \cdot \vec{u_j}| > 0.8$. A typical snapshot of such a droplet, formed by 330 spherocylinders, is shown in Figure 4.4. This snapshot was obtained for a system, indicated by a triangle in Figure 4.3 ($\nu_{\rm r} = 0.09$, $\nu_{\rm sp} = 0.28$).

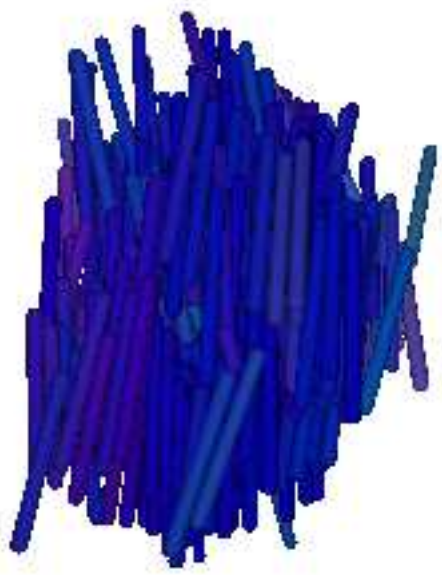

Figure 4.4: A snapshot of a droplet formed by 330 spherocylinders in a system with $\nu_{\rm r} = 0.09$ and $\nu_{\rm sp} = 0.28$ (a view from the side, the nematic total director is vertical). The particles are colour-coded according to their orientations.

All the droplets which we obtain in these simulations turn out to be relatively big with respect to the simulation box and, thus, can interact with themselves via the periodic boundaries. This means that one has to investigate systems with a smaller volume fraction of the nematic phase and larger simulation boxes. However, equilibrating such systems is quite problematic because one needs a lot of computation time. An efficient way for solving this problem was proposed in [96, 97] for a system of a nanocrystal in a barostat, which was created by particles that do not interact with each other but interact with the nanoparticles with a repulsive potential that prevents gas particles from penetrating the nanocrystal. In such a system, non-interacting

particles far enough from the crystal form an ideal gas, this fact was used in order to avoid simulating the whole pressure bath with periodic boundary conditions. Instead of that only gas particles in the vicinity of the crystal were considered - when the crystal moved, distant gas particles were removed and new gas regions were created.

4.2 Rods and spheres of different diameters

4.2.1 Model and simulation details

Now we consider droplets of hard spherocylinders (see Chapter 2), which we stabilize by surrounding them by a gas of spheres with a diameter twice that of the thickness of the spherocylinders, $D_{\mathrm{sp}} = 2D$ (Figure 4.5).

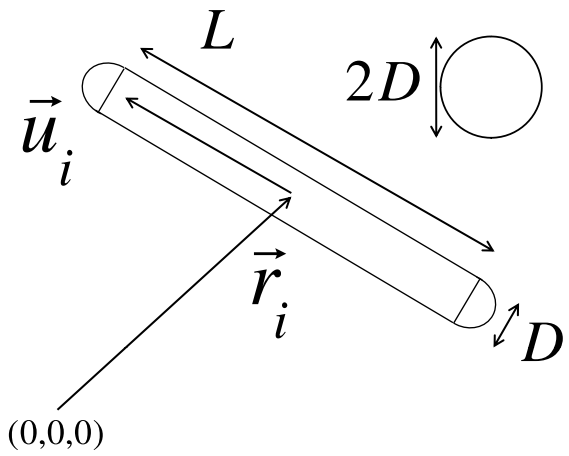

Figure 4.5: Sketch to introduce definitions: Each spherocylinder consists of a cylinder of length L and diameter D capped by two hemispheres of diameter D. The location of the i-th spherocylinder is given by its centre of mass vector $\vec{r}_i$ and the orientational unit vector $\vec{u}_i$. The spheres of diameter $D_{\mathrm{sp}} = 2D$ are hard with respect to spherocylinders and freely interpenetrable among each other.

Like in the previous model (see Section 4.1.1), the spherocylinders interact via a hard-core repulsion, while the spheres interact with a

hard-core repulsion with spherocylinders but are able to freely interpenetrate each other at no energy cost. We consider such concentrations of particles that produce a very strong phase separation into sphere- and rod-rich phases, so the former behaves as a (nearly) ideal gas of spheres that in essence acts as a barostat for the droplet consisting of almost only spherocylinders.

As it was already mentioned above, this implies that by means of changing the number of spheres in the system at a fixed volume, we can tune the pressure exerted on the rods in the droplet. Through that we vary density of the drop and therefore also the physical properties of the drop, such as the elastic response if the drop is in a nematic fluid state. Hence, we use the number density of spheres ρ_{sp} (note, that we use D as the unit length) measured far away from the droplet as a parameter that characterizes the external conditions imposed on the droplets formed. The same method has been used in an earlier study of the formation of nanocrystals in a simulation [100].

The simulations were performed at fixed particle number N and simulation box volume V (and temperature T, but as the system is purely entropic, temperature is not relevant here) in a cubic box with periodic boundary conditions. We focus on spherocylinders with an aspect ratio of $L/D + 1 = 11$ (i.e. $L/D = 10$), and spheres with a diameter twice that of the thickness of the rods, because spheres that are much larger than this introduce strong effects on the surface anchoring, whilst for smaller spheres the numbers needed in the simulation turn out to be unpractical from a computational point of view (see Chapter 4.1).

The number of spherocylinders in the box, N_{r}, was varied from 200 to 700, and the number of spheres was fixed such that phase separation was induced into two phases containing virtually only spherocylinders or spheres. This corresponded in our simulations to between approximately 20000 and 70000 spheres. One can be confused by

the fact, that the amount of spheres in the simulation was sometimes even larger than in the previous part (see Section 4.1), which in turn could lead to long equilibration times. However, this was not the case, because most of the time during simulation is used for checking possible overlaps between the neighbouring particles. From the fact that the spheres in this model can freely interpenetrate each other follows that in the case of a very strong phase separation into nematic and isotropic phases (with only few spherocylinders present in the latter one) the simulation times are reduced with respect to the case when both phases contain many spherocylinders.

We chose the simulation box to be $70^3 D^3$, i.e., sufficiently large to ensure that the spherocylinders did not interact directly with each other via the periodic boundaries. We verified the droplets that form are not system spanning. The systems were equilibrated by local translation and rotation moves. Depending on the specific concentrations, $10^6 - 10^7$ MC sweeps were required.

The boundary and volume of a droplet is established as follows: We first divide the system into small boxes and next verify whether a box contains the center of a sphere or whether it is intersected by any spherocylinder. In the latter case, this box is counted as a part of the droplet. If it so happens that a box does not fall into either of the two categories, it is counted as a part of the droplet if it has a larger number of nearest neighboring boxes containing spherocylinders than spheres.

For a proper averaging of observables in addition to rotation of the configurations in such a way that the director always points in the same direction (see Sec.2.5) we make a translational shift of the configurations in such a way that the centers of masses of the obtained droplets coincide.

4.2.2 Results and discussion

In Figure 4.6 we present the "shape" diagram of hard spherocylinder droplets immersed in a gas of spherical particles, which we obtained in our simulations. The horizontal axis shows the volume of the droplet of spherocylinders in units of cylinder thickness cubed, D^3, and the vertical axis the number density of the spheres far away from the droplet. We indicate with asterisks the system conditions for which we ran the simulations. The letters "a" through "l" are used in the following to refer to specific points in this diagram. We have indicated schematically in the figure the shape and the internal structure of the droplets, which we discuss in more detail below. The numbers in the boxes indicate the aspect ratios of the droplets, obtained from the density profiles.

Figures 4.7 and 4.8 give the snapshots of two typical structures which correspond to the systems "i" and "c", respectively. In these figures only the spherocylinders are shown for clarity. One can see two essential differences between these structures: The first of the two droplets shown is i) more elongated and ii) the spherocylinders in this droplet have a much stronger tendency to orient in one direction. Below we will analyse these effects in a more quantitative fashion.

The difference between these droplets is caused by the difference in bulk sphere density and hence osmotic stress imposed on the droplet by the sphere gas. Droplet "i" is subject to much higher pressure and hence is condensed much more than droplet "c", and has crossed over to the nematic phase. The rod densities ρD^3 in the two drops are 0.034 and 0.027 (averaged over each droplet), respectively. From the Lee-Parsons theory of the nematic transition in bulk fluids of hard rods [101], we expect for spherocylinders of aspect ratio $L + D = 11$ the nematic transition to occur at a pressure of $PD^3/k_BT \approx 0.25$, corresponding to an ideal gas density of $\rho_{\rm sp}D^3 \approx 0.25$. This is in

reasonable agreement with the transitional regime around $\rho_{\rm sp}D^3 \approx 0.23$ in the diagram. We also estimated the transition density by simulating a compression curve and an expansion curve in the bulk and obtained $\rho_{\rm sp}D^3 \approx 0.22$, which again is in good agreement with the numbers above. We note that due to the effects of Laplace pressure the nematic transition should occur at a somewhat lower sphere density than that in bulk solution. For details we refer to the Appendix.

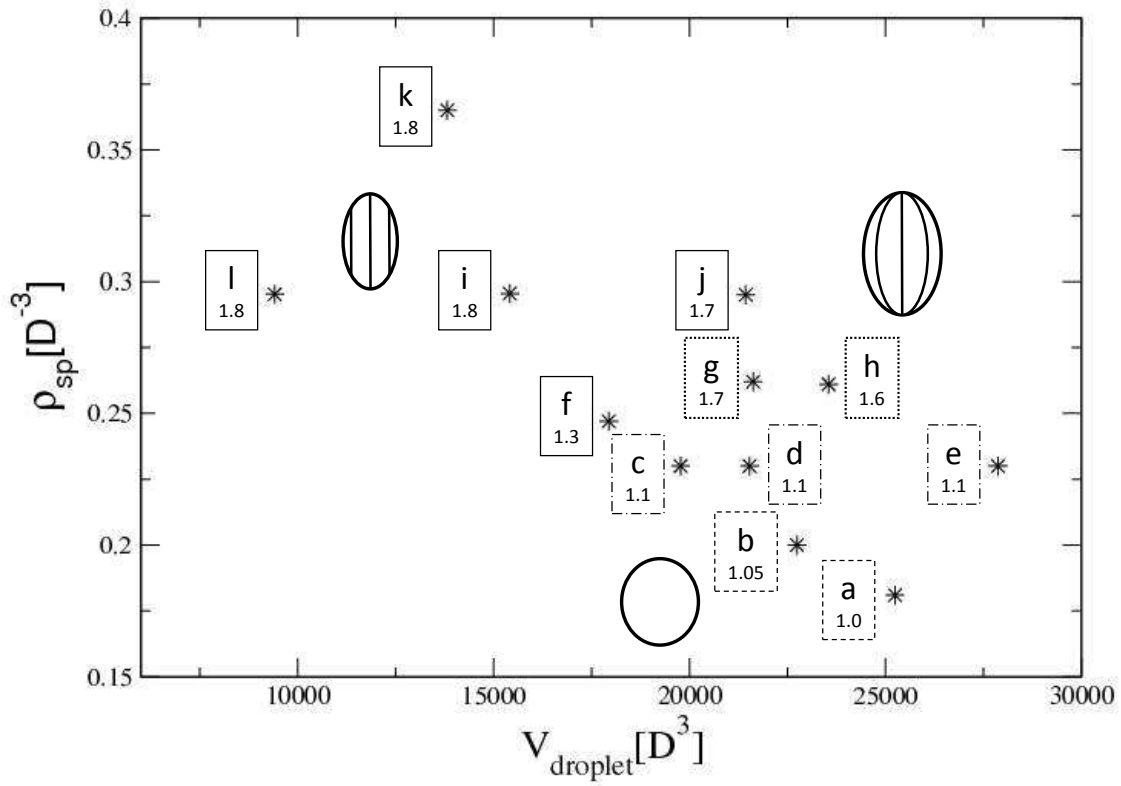

Figure 4.6: "Shape" diagram of hard spherocylinder droplets immersed in a gas of spherical particles. The horizontal axis shows the volume of the droplet of spherocylinders in units of cylinder thickness cubed, D^3, and the vertical axis the number density of the spheres far away from the droplet. The letters "a" to "l" are used in the main text to refer to specific points on the diagram. The sketches show schematically the shape and the internal structure of the droplets, and distinguish spherical isotropic droplets, elongated nematic droplets with either a homogeneous or a bipolar director field. The numbers in the boxes indicate the aspect ratios of the droplets. The boundaries of the boxes distinguish between: isotropic (dashed), transition region (dash-dotted), bipolar (dotted) and homogeneous (solid).

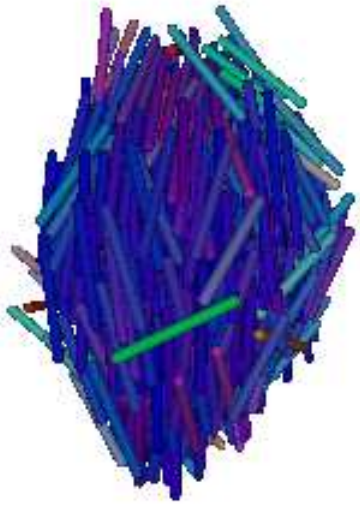

Figure 4.7: A snapshot of a nematic droplet of rods that forms for the conditions indicated by "i" in Figure 4.6. The spherical particles are not shown for clarity. The nematic total director is vertical. The average rod density in the drop is equal to $\rho D^3 = 0.034$.

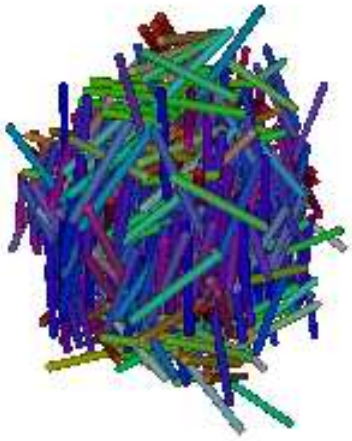

Figure 4.8: A snapshot of an almost isotropic droplet of rods for conditions "c". The average rod density in the drop is equal to $\rho D^3 = 0.027$.

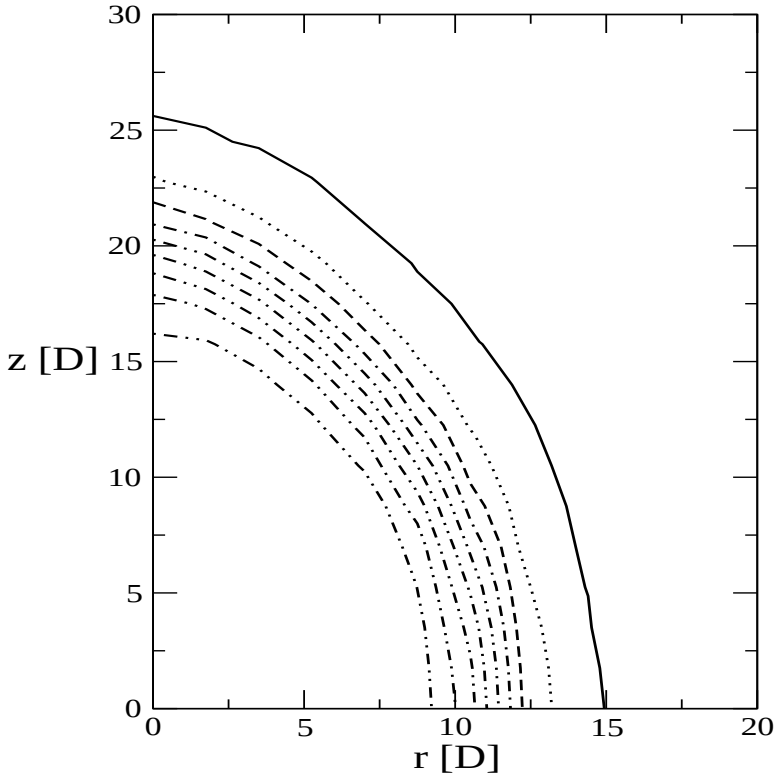

Figure 4.9: Isodensity lines of spherocylinders in a droplet from conditions "i", shown in cylindrical coordinates. The solid line marks the boundary of the drop. Successive dashed, dash-dotted, etc., lines demarcate densities from $\rho D^3 = 0.039$ to $\rho D^3 = 0$.

In Figure 4.9 we have plotted a typical iso-density distribution in the r-z-plane for nematic droplet "i" (here and in the following text r is used instead of r_{xy} for simplicity). Inside the droplet the spherocylinders have an approximately constant rod density equal to $\rho D^3 = 0.039$, which rapidly decays when approaching the interface to the gas of spheres. It is clear that the drop is not spherical, the aspect ratio being approximately 1.8. For comparison, and in order to determine the shape of the droplets, we cut a slice from the $r - z$-density profile at half of its maximum value. That is where we expect the Gibbs surface to be situated. The curves obtained in this way are shown in Figure 4.10 for several systems corresponding to the points "a", "b", "c", "f", "i", and "k". These systems consist of the same amount or

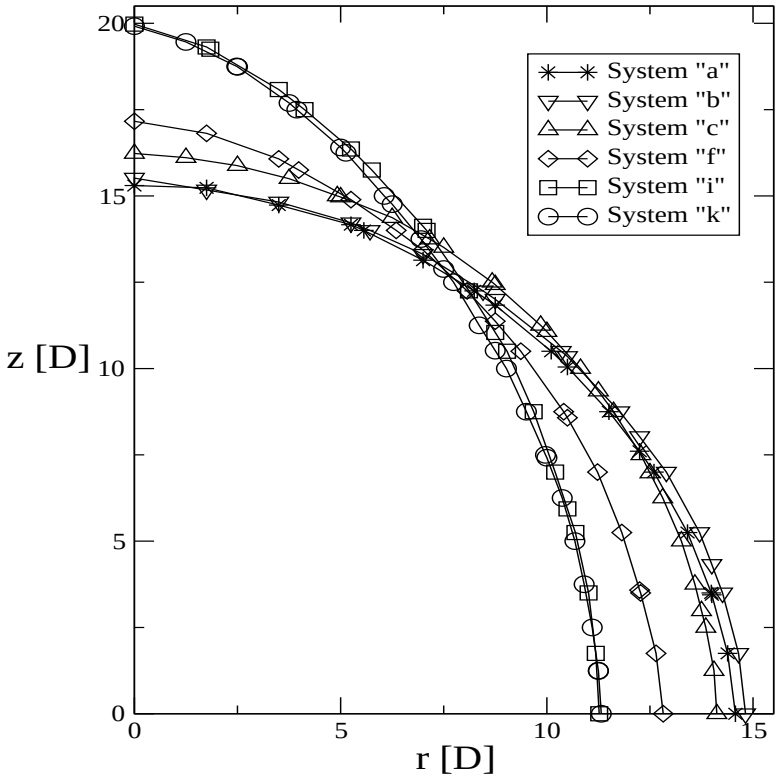

Figure 4.10: The shapes of droplets consisting of 500 spherocylinders at different pressures of spheres (conditions "a", "b", "c", "f", "i", and "k" indicated in the schematic of Figure 4.6). Droplets "a" and "b" are those of isotropically oriented rods, and hence more or less spherical. Drop "c" is in the transition zone from the isotropic to the nematic state. Drops "f", "i" and "k" are nematic drops, with "i" and "k" exhibiting more or less uniform director fields and "f" a more bipolar one.

spherocylinders ($N_{\mathrm{r}} = 500$) but have various densities of spheres.

At low pressures the droplets are spherical on average. This is to be expected if the rods are in their isotropic state. However, if the pressure is increased the droplets crossover to the nematic phase and hence become elongated in order to reduce either the elastic deformation of the director field if the anchoring is strong, or the anchoring free energy if the anchoring is weak. As already advertised, the crossover occurs when the typical drop dimension exceeds the healing length, which we are going to discuss in more depth in the following section.

On increase of the density of rods, the elastic constants in all likelihood increase, too, as should the interfacial tension and potentially also the anchoring strength. We expect from scaling arguments that the ratio of the anchoring strength and the surface tension is a weak function of the pressure [102], however, and in the weak anchoring regime it is this ratio that dictates the aspect ratio of the drops [56]. In the strong anchoring regime the aspect ratio is an increasing function of the healing length that in the equal-constant approximation is given by the ratio of the elastic constant and the surface tension. Hence, whether the droplets become more elongated then depends on how strongly these two energies depend on the pressure. Apparently, the elastic constants increase more strongly with pressure because the aspect ratio increases from about 1.1 to 1.8 with increasing sphere concentration.

We observe the same tendency for the systems of 700 spherocylinders. At low pressures the droplet is more or less spherical (state point "e", aspect ratio 1.1) and at high pressures the droplet becomes elongated (state point "j", aspect ratio 1.7). We have to note, however, that the droplet size also affects the aspect ratio: it decreases with increasing the size. This has been observed experimentally and is predicted theoretically based on macroscopic theory [82, 58, 81]. The aspect ratios for all the state points are shown in the boxes in the "shape" diagram in Figure 4.6, with an estimated error of 0.1 for the nematic droplets.

One has to point out that the shape of the "spherical" droplets is spherical only on average. The elongation of isotropic droplets is random, in contrast to nematic droplets where it is related to an orientational order and thus the information about it is not lost while accumulating the density profiles. So, in the case of isotropic droplets the shape has to be analysed separately for each configuration.

In order to do this we calculate and diagonalise the matrix of inertia

of a given droplet

$$I = \sum_{i=1}^{N_r} \begin{pmatrix} {y_i}^2 + {z_i}^2 & -xy & -xz \\ -xy & {x_i}^2 + {z_i}^2 & -yz \\ -xz & -yz & {x_i}^2 + {y_i}^2 \end{pmatrix}, \tag{4.2}$$

where x_i, y_i and z_i are the components of the center of mass vector $\vec{r_i}$. In order to obtain information about the elongation of the droplets we assume at this point that they are ellipsoids of uniform density, for which the eigenvalues of the matrix of inertia are known:

$$I_{xx} = m\frac{b^2 + c^2}{5}, \quad I_{yy} = m\frac{c^2 + a^2}{5}, \quad I_{zz} = m\frac{a^2 + b^2}{5}, \tag{4.3}$$

here a, b and c are the radii along the x,y and z axes, respectively, and m is the mass of the ellipsoid.

Following this assumption, we calculate the three radii for each configuration of a given system, then the ratios of the largest and smallest radii to the middle one, and average them over all the configurations. These ratios for all the investigated systems are presented in Table 4.1. As one could expect, the aspect ratios of the droplets in a high-density regime correspond well to the values, obtained from the analysis of the density profiles. The nematic droplets are elongated in the direction of the nematic field (this was seen on the visualised snapshots and was proven by the fact that fluctuations between the nematic director and the eigenvector of the maximum value of the matrix of inertia were

Table 4.1: Aspect ratios of the droplets obtained from the matrix of inertia.

System	c/b	a/b	System	c/b	a/b
"a", "b"	1.1 ± 0.1	0.9 ± 0.1	"h"	1.51 ± 0.05	0.90 ± 0.05
"c" - "e"	1.1 ± 0.1	0.9 ± 0.1	"i", "l"	1.68 ± 0.05	0.92 ± 0.05
"f"	1.2 ± 0.1	0.8 ± 0.1	"j"	1.62 ± 0.05	0.92 ± 0.05
"g"	1.61 ± 0.05	0.88 ± 0.05	"k"	1.75 ± 0.05	0.95 ± 0.05

negligible). In the case of the "spherical" droplets one sees that their axes fluctuate significantly. This means that these droplets are not always spherical, and any given snapshot of such a droplet is deformed considerably.

We now turn to the orientational state of the rods in the droplets. This is described in terms of the eigenvalues of the orientational tensor $\mathbf{Q}$ (see Section 4.2.1). In Figure 4.11 we show the r- and z-profiles of these eigenvalues for the droplets "i", "f", and "c" (each of those consists of 500 spherocylinders). The droplets become less ordered and less elongated. Droplet "i" has a high nematic ordering in its center, which slightly decays on approach of the interface to the gas of spheres in both, the r- and the z-direction. Droplet "f" has a lower

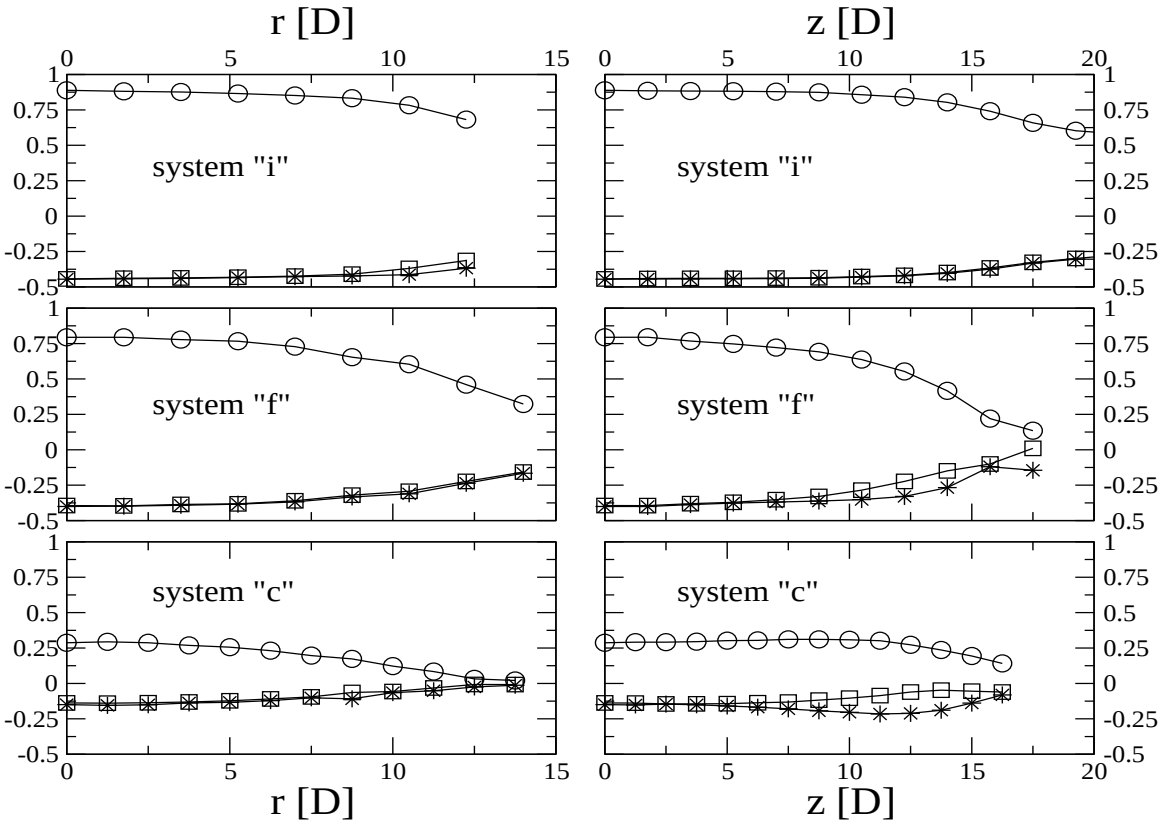

Figure 4.11: The r- and z-profiles of the eigenvalues of the orientational tensor $\mathbf{Q}$ for the systems "i", "f", and "c" (each consisting of 500 spherocylinders).

density and also a nematic order parameter that is smaller. Droplet "c" has even lower values of the nematic order parameter, and at the interfaces all the eigenvalues become equal to zero, indicating an isotropic configuration. This drop probably is close to the conditions where the isotropic-nematic transition takes place.

By analysing the tensor **Q** for all the investigated droplets, we construct scalar order parameter profiles as well as the nematic director-field configuration. The results are indicated schematically in the diagram in Figure 4.6:

1) Droplets "a" and "b" are "spherical" droplets of an isotropic rod fluid;

2) Droplets "c", "d" and "e" are in the isotropic-nematic transition region, exhibiting a strongly fluctuating orientational order;

3) States "f" to "l" are strongly nematic drops;

4) The director field of drops "i", "j", "k" and "l" is more or less uniform, those of "g" and"h" bipolar, and of "f" in between these two.

To illustrate these findings, we show the director field (the axis given by the eigenvector corresponding to the largest eigenvalue of the orientation tensor) as a function of the radial and axial distances r and z in Figure 4.12 for the case "k" and in Figure 4.13 for the case "h". The director field of the tactoid "k" is more or less uniform and oriented along the main axis of the drop. That of "h" is bipolar, i.e., curved along the elongated drop surface toward the tips, where the scalar order parameter drops to zero. This signifies the melting of the nematic near the tips, where theoretically one would expect the surface point defects ("boojums") to reside [56].

The director field in a nematic droplet is determined by the interplay of surface anchoring and elastic forces. The bipolar structure can

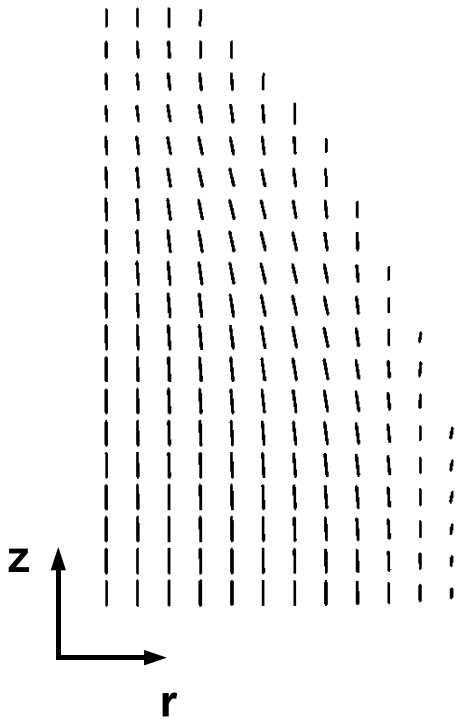

Figure 4.12: An example of a nematic droplet with a homogeneous director field (system "k"), the eigenvectors corresponding to the maximum eigenvalues of the orientational tensor $\mathbf{Q}$ are shown in polar coordinates.

only be formed if the energy for bending is small enough compared to the surface energy. This can be achieved if the density of the suspension is small (but the droplet still has a nematic structure), or if the droplet is big (and, therefore, the curvature of the interface is small). Systems "g" and "h" fit into this category.

The aspect ratio of the droplets does not depend on their size if the director field inside the droplets is homogeneous. This follows directly from the Wulff construction of the droplet shape given any polar angle-dependent surface tension [56]. Indeed, all the droplets with an approximately homogeneous director field, droplets "i", "j", "k", and "l", that we obtained in our simulations have approximately the same aspect ratio within a statistical error of the simulation of

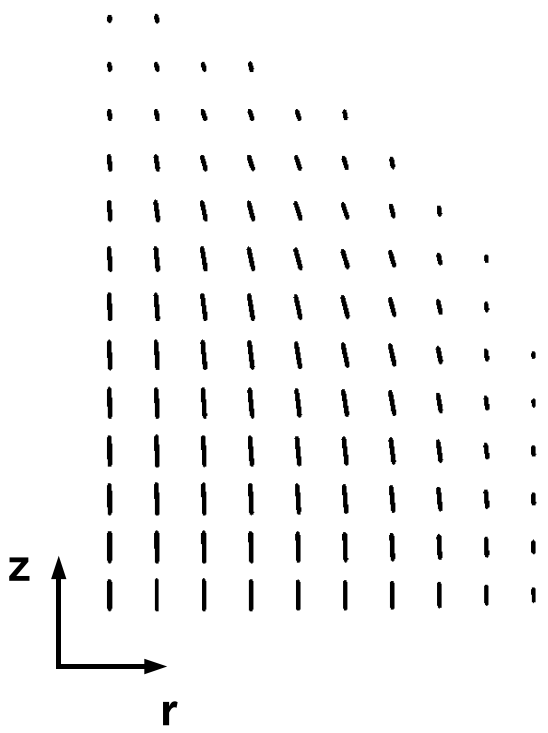

Figure 4.13: An example of a nematic droplet with a bipolar director field (system "h"), the eigenvectors corresponding to the maximum eigenvalues of the orientational tensor $\mathbf{Q}$ are shown in polar coordinates.

about 0.1, in agreement with this theoretical prediction. From the aspect ratio observed in the simulations (we use the value 1.8) we can in fact deduce a dimensionless anchoring strength. Let us presume that the anisotropic surface tension γ has a functional form of the Rapini-Papoular type [103], so $\gamma = \tau[1 + \omega(\vec{q} \cdot \vec{n})^2]$, with τ the bare surface tension, ω the dimensionless anchoring strength, $\vec{q}$ the surface normal and $\vec{n}$ the director field at the surface of the drop. For planar anchoring to be favored, $\omega > 0$. From the Wulff construction we then deduce that the aspect ratio of the drop equals $1+\omega$ for $0 \leq \omega \leq 1$ and $2\sqrt{\omega}$ for $\omega > 1$ [56]. Hence, we find from our simulations a value for ω of 0.8, quite close the value of 0.65 found by Dijkstra and co-workers in a simulation study of nematic drops nucleated in a super-saturated

dispersion of hard rods [104].

According to the macroscopic theory [57] from the crossover from bipolar to homogeneous director fields depends on three dimensionless groups: the anchoring strength, the ratio of the elastic constants $K_{33}/(K_{11} - K_{24})$ (here K_{11} denotes the splay elastic constant, K_{33} denotes the bend elastic constand, and K_{24} the saddle-splay surface elastic constant), and the dimensionless volume $V_{droplet}/\lambda^3$, where $\lambda \equiv (K_{11} - K_{24})/\tau\omega$ is the so-called healing length, which measures the scale below which the director field "resists" deformation by the coupling to the interface. According to Figure 4.6, the crossover occurs for drops of a volume about $1.7 \times 10^4 D^3$ for our model. This value may actually depend on the sphere density, but because of the lack of any detailed information we shall ignore this for simplicity. Presuming that the bend elastic constant is about ten times larger than the splay elastic constant, which seems reasonable on account of predictions for hard rods in the Onsager limit, the crossover occurs at a droplet volume equal to about ten times the healing length cubed [57, 58]. So, we find for the healing length $\lambda \approx 12D$, which is about a rod length. Clearly, macroscopic theories, such as those of Kaznacheev and collaborators [82, 84], and of Prinsen and van der Schoot [56, 57, 58], could be expected to break down at such small length scales, yet the predicted crossover from uniform to bipolar director fields apparently still survives.

From the estimate of the healing length, we can obtain an order of magnitude estimate of the interfacial tension between the rods and the spheres that we can compare with the scaling estimate given in the Appendix. If we presume the Saupe-Nehring relation to hold, implying that $K_{24} = (K_{11} - K_{22})/2$ [105], and make use of the approximate expression $K_{22} = K_{11}/3$ [106], we obtain $\lambda \approx 2K_{11}/3\tau\omega$. Hence, $K_{11}/\tau \approx 14D$, or, $\beta\tau D^2 \approx \beta K_{11} D/14$, where β is defined as the inverse thermal energy $1/k_B T$. Within a second-virial approximation,

which admittedly is not very accurate for rods of aspect ratio below 20, we expect $\beta K_{11} D \approx 0.9$ to hold near the transition [107]. Hence, for the interfacial tension between the rods and the spheres we obtain the estimate $\beta\tau D^2 \approx 0.07$. According to our scaling estimate cited in the Appendix, we have $\beta\tau D^2 \approx 0.25\alpha\xi/D$ with α a prefactor that should be of order 0.1 [102] and ξ the interfacial width. If $\xi \approx L$, this then implies that $\alpha \approx 0.03$, which is somewhat smaller than expected [102].

In order to go beyond this qualitative analysis, simulation data of the elastic constants of the bulk nematic and of the surface tension between the co-existing bulk fluids would be necessary. Unfortunately, these are not available yet for spherocylinders of aspect ratio 11, as, in particular, simulations to determine elastic constants are computationally rather expensive. (To our knowledge, elastic constants have been computed only for spherocylinders of aspect ratio 6 [108].)

4.2.3 Summary

In this chapter, an extenstion of the Asakura-Oosawa-Vrij model for colloid-polymer mixtures to anisotropic colloids was considered. The main focus was made on the droplets of rods which were formed under certain conditions.

First, we investigated systems of hard spherocylinders of length $L/D = 10$ and spheres of the same diameter with various total densities of both components. We performed Monte Carlo simulations in the NVT-ensemble, equillibrating the system by means of local (translational and rotational) moves of single particles and by cluster moves. In all the investigated systems we observed demixing into sphere-rich and spherocylinder-rich phases, the latter one forming either a layer, a tube or a droplet. All the droplets which we obtained in these simulations were relatively big with respect to the simulation box and,

thus, could interact with themselves via the periodic boundaries.

Then we considered mixtures spherocylinders ($L/D = 10$) and spheres of twice larger diameter ($D_{\mathrm{sp}} = 2D$) with such concentrations of particles that a very strong phase separation into sphere- and rod-rich phases occured, the latter one forming a droplet and the former one in essence acting as a barostat for it.

We investigated such systems with various densities of the components and have shown that these droplets of hard rods, osmotically compressed by the presence of spherical particles, undergo an isotropic-nematic transition at sufficiently high osmotic stress. We analysed the shapes the droplets and found that the isotropic droplets are spherical on average, but any given configuration can be deformed considerably. We found the nematic droplets not to be spherical but elongated in the direction of the nematic director. The director field of the drops is uniform if smaller than a critical size and bipolar if larger than that. We interpret our findings in terms of the predictions of continuum mechanical theory that minimizes the combined effect of an elastic deformation of the director field and an anchoring frustration of this director field at the surface of the drops. Although in our simulations the drops are not at all large on the scale of the rods, and continuum theory should perhaps not be expected to be accurate, results from both levels of description seem to be consistent with each other down to drop sizes that are as small as a few times the particle length.

Chapter 5

Final remarks

This work is focused on various properties of isotropic and nematic colloidal droplets. The colloidal particles were modeled as hard spherocylinders. Two different types of systems have been considered: in the first one spherocylinders were confined into a spherical cavity, while in the second one droplets of rods were formed by means of osmotic compression caused by spherical particles that acted as depletion agents.

First, we investigated effects of ordering of a liquid of rods near hard curved walls. In particular, we studied how adsorption and orientational ordering depend on the curvature of the wall and on the density of the liquid. The results which we obtain are consistent with results of previous computer simulation studies and theoretical approaches.

In nematic systems of rods confined to a cavity, both elastic deformations and surface ordering take place: on the one hand, the surface of the cavity orients the director field ("surface anchoring"), on the other hand deformations of the director field cost elastic energy. Hence the equilibrium director field is determined by a compromise between surface anchoring and elasticity. In our simulations, all the nematic systems formed bipolar structures. This leads us to a conclusion that for such a model the energetic contribution due to anchoring

strength is always larger than the energetic contribution due to elasticity. Bipolar structures, which we observed, differed from ideal ones with boojums at the poles. We performed only qualitative analysis of these defects, because of very strong fluctuations due to small sizes of the considered systems. This means that the presented work can be extended in the future, because simulation of larger systems will allow to analyze the structure of the defects in a much more detailed way.

As a next step, we considered an extension of the Asakura-Oosawa-Vrij model for colloid-polymer mixtures to anisotropic colloids. First, we investigated systems of hard spherocylinders of length $L/D = 10$ and spheres of the same diameter. Though under certain conditions we obtained droplets of rods surrounded by a sphere-rich phase, we did not perform detailed analysis of these droplets, because the ones which we could equilibrate were rather large with respect to the size of the simulation box and, thus, their properties would be affected by the periodic boundaries. However, it should be possible to investigate the properties of such droplets when it becomes possible to perform computer simulations faster.

Then, we proceeded with a slightly different model with the same rods but spheres of twice large diameter. In such a system demixing into virtually pure phases occurs at considerably lower number densities of the species. Due to this fact we could equilibrate droplets of rods in sufficiently large boxes. The gas of spheres in such a system works as a barostat for the droplet and by varying the density of the spheres one changes the effective pressure.

We found that at sufficiently high osmotic pressures the droplets formed by rods have nematic structure. Such droplets are elongated, resulting from the competition between the anisotropic surface tension and the elastic deformation of the director field. In agreement with recent theoretical predictions we found that sufficiently small tactoids have a uniform director field, whilst large ones are charac-

terized by a bipolar director field. At lower pressures the droplets are isotropic and almost spherical, however, their shape fluctuates significantly. We interpreted our results in terms of predictions of the continuum mechanical theory, and even though the relevant length scales in our simulations are rather small the estimate of the surface anchoring strength which we got seems to be quite reasonable.

Appendix A

Adsorption on a curved wall

In Figure A.1 we show the obtained dependence of adsorption Γ (see Section 3.2) on $\ln(\rho_{\mathrm{i}} - \rho_{\mathrm{b}})/\rho_{\mathrm{i}}$ for a system of hard spherocylinders of length $L = 15$ confined into a spherical cavity of radius $R/L = 2$.

Fitting $\Gamma = a_0 + a_1 \ln((\rho_{\mathrm{i}} - \rho_{\mathrm{b}})/\rho_{\mathrm{i}})$ for the region $(0.03 < (\rho_{\mathrm{i}} - \rho_{\mathrm{b}})/\rho_{\mathrm{i}} < 0.10)$ we find $a_0 = -0.28$ and $a_1 = -0.14$.

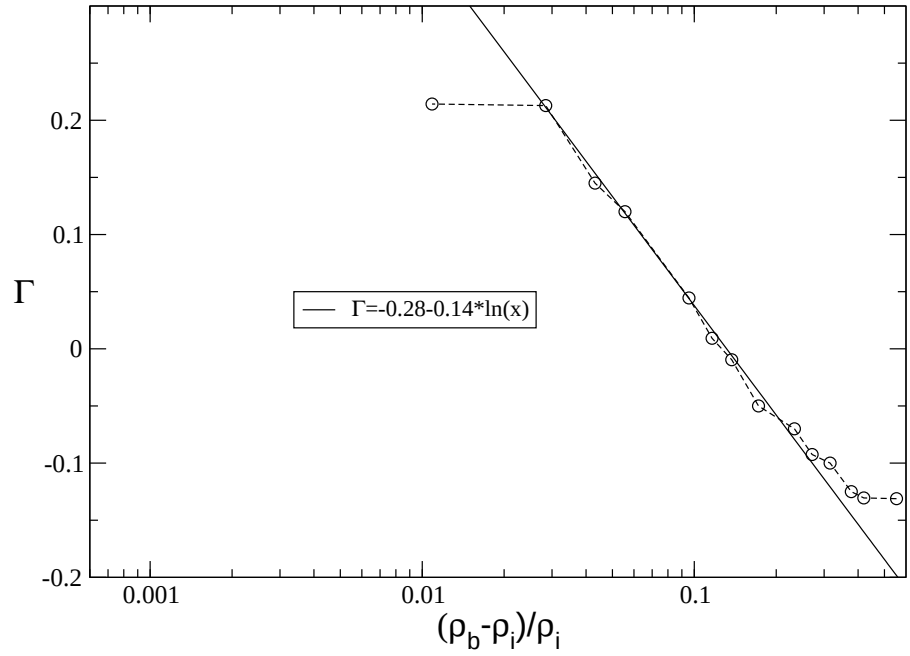

Figure A.1: Adsorption Γ versus $(\rho_{\mathrm{i}} - \rho_{\mathrm{b}})/\rho_{\mathrm{i}}$ for a system of hard spherocylinders of length $L = 15$ confined into a spherical cavity of radius $R/L = 2$.

Appendix B

Defects in nematic droplets

Here we present additional data on the defects on the poles of nematic spheres of radii $R/L = 2$ and 2.5 with $\rho_b = 4.55$ (see Section 3.3). Figures B.1 and B.3 show the dependences of the eigenvalues of the orientational tensor $\mathbf{Q}$ of the particles lying on the z-axis of the system (which is defined as the orientation of the overall nematic director field) on the distance from the pole of the sphere. From the graph one can conclude that there is a highly ordered nematic phase in the centre of the sphere. While approaching the wall the nematic order parameter decays until it reaches its minimum at $z \sim L/5$ and $z \sim L/3$ (for $R/L = 2$ and 2.5, respectively). At the same time the difference between λ_- and λ_0 starts growing, indicating a presence of a biaxial structure.

In Figures B.2 and B.4 typical snapshots of the defects in the systems ($R/L = 2$ and 2.5, respectively) are presented. We see the same structure as in the system with $R/L = 3.03$ (see discussion in Section 3.3).

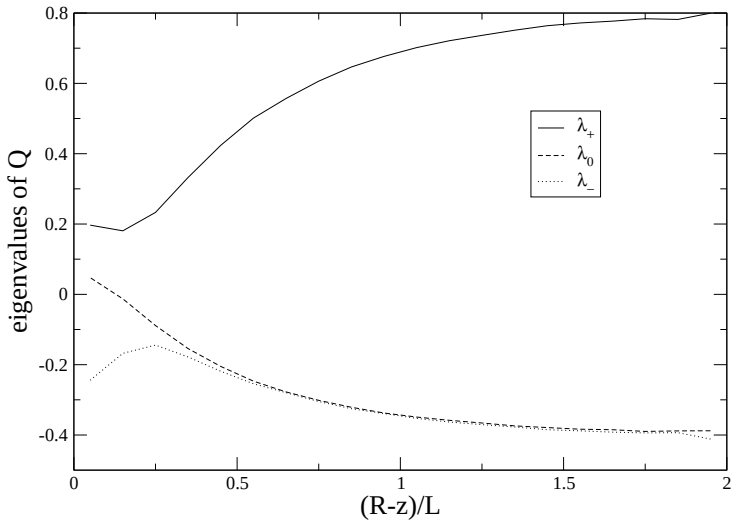

Figure B.1: Eigenvalues of the orientational tensor $\mathbf{Q}$ for the particles lying on the z-axis of the system versus the distance from the pole of the sphere. The radius of the confining sphere R/L is equal to 2.

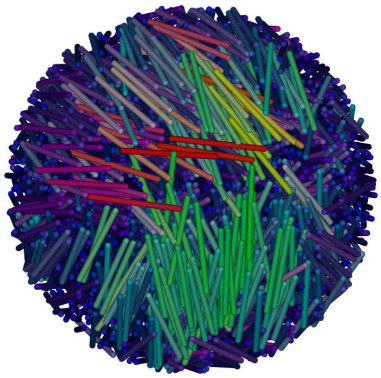

Figure B.2: A typical snapshot of a pole of the sphere ($R/L = 2$). The particles are colour-coded according to their orientations.

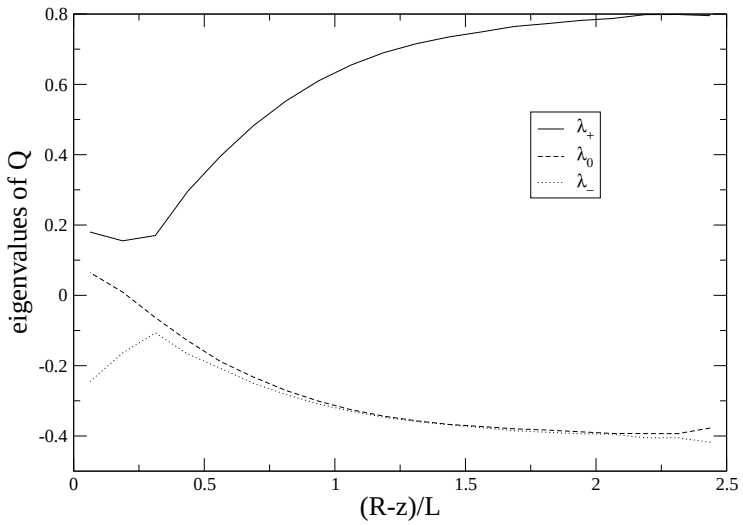

Figure B.3: Eigenvalues of the orientational tensor $\mathbf{Q}$ for the particles lying on the z-axis of the system versus the distance from the pole of the sphere. The radius of the confining sphere R/L is equal to 2.5.

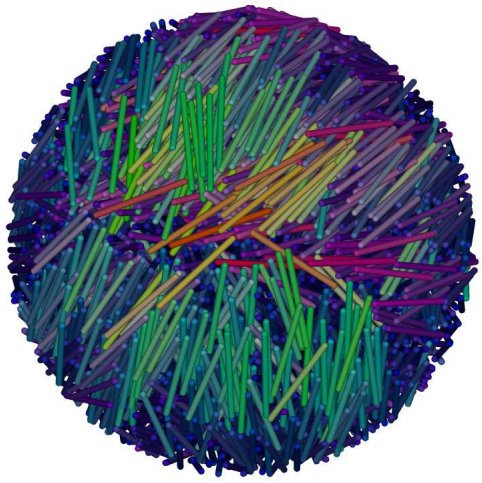

Figure B.4: A typical snapshot of a pole of the sphere ($R/L = 2.5$). The particles are colour-coded according to their orientations.

Appendix C

Laplace pressure

An estimate for the rod density in the droplet as a function of the number N of rods and the density of spheres ρ_{sp} can be obtained by presuming complete demixing of the two components and by presuming that the interface between them is sharp. Let R be the radius of the drop, assumed perfectly spherical, then $\rho = 3N/4\pi R^3$ is the density of the rods in drop. The bulk pressure of the hard rods is to a very good approximation equal to the expression put forward by Parsons and by Lee [109]

$$\beta P = \rho \left(1 + \frac{2\phi(2-\phi)}{(1-\phi)^3} \left[1 + \frac{3\pi}{8} \Lambda \right] \right),$$

at least in the isotropic phase, where $\phi = \rho(\pi D^3/6 + \pi L D^2/4)$ denotes the packing fraction, $\Lambda = (L/D)^2/\pi(1 + 3L/2D)$ for slender rods is proportional to their aspect ratio and β denotes the inverse thermal energy $1/k_B T$ with k_B Boltzmann's constant and T the absolute temperature. The pressure of the ideal gas of spheres obeys

$$\beta P_{\mathrm{sp}} = \rho_{\mathrm{sp}}.$$

Mechanical equilibrium between the gas of hard rods and that of ideal spheres demands that

$$P - \frac{2\gamma}{R} = P_{\rm sp},$$

where the second term on the left-hand side is the contribution from the Laplace pressure across the curved interface, with γ the interfacial tension that presumably depends on the bulk densities of both the rods and the spheres. For any given number of rods N, this equation sets the equilibrium size of the drop.

An estimate of the magnitude of the Laplace pressure may be given by making use of the scaling Ansatz $\gamma \approx P_{\rm sp}\xi$, with $\xi \approx L$ the actual interfacial width [102]. Hence, $P/P_{\rm sp} \approx 1 + 2\alpha\xi/R$ with α a constant of proportionality that we estimate to be of order 0.1 [102]. So, the presence of the interface increases the pressure in the drop relative to that in the reservoir of spheres and hence induces the onset of the nematic phase at lower densities of spheres the smaller the drop.

From Table I of Lee [110], we deduce by linear interpolation that for rods of $L/D = 10$ the bulk nematic phase sets in at a dimensionless pressure $\beta P D^3 \approx 0.247$, corresponding to a sphere fraction of $\rho_{\rm sp} D^3 \approx 0.247$, in reasonable agreement with what we find in the simulations (see Figure 4.6).

List of Figures

Bibliography

[1] D. F. Evans and H. Wennerstrøm. *The colloidal Domain - Where Physics, Chemistry, Biology, and Technology Meet.* VCH Publishers, New York, 1999.

[2] P. G. de Gennes and J. Prost. *The Physics of Liquid Crystals.* Clarendon Press, Oxford, 1993.

[3] Z. Dogic and S. Fraden. Ordered phases of filamentous viruses. *Curr. Opin. Colloid Interface Sci.*, 11:47, 2006.

[4] P. Davidson and J. C. P. Gabriel. Mineral liquid crystals. *Curr. Opin. Colloid Interface Sci.*, 9:377, 2005.

[5] J. Käs, H. Strey, J. X. Tang, D. Finger, R. Ezzell, E. Sackmann, and P. A. Janmey. F-actin, a model polymer for semiflexible chains in dilute, semidilute, and liquid crystalline solutions. *Biophys. J.*, 70:609, 1996.

[6] S. Zhang and S. Kumar. Carbon nanotubes as liquid crystals. *Small*, 4:1270, 2008.

[7] G. J. Vroege and H. N. W. Lekkerkerker. Phase transitions in lyotropic colloidal and polymer liquid crystals. *Rep. Progr. Phys.*, 55:1241, 1992.

[8] H. Zocher. Spontaneous structure formation in sols; a new kind of anisotropic liquid media. *Z. Anorg. Chem.*, 147:91, 1925.

[9] F. C. Bawden, N. W. Pirie, J. D. Bernal, and I. Fankuchen. Liquid crystalline substances from virus-infected plants. *Nature (London)*, 138:1051, 1936.

[10] P. G. Bolhuis. *Liquid-like behavior in solids. Solid-like behavior in liquids.* PhD thesis, Netherlands, 1996.

[11] L. Onsager. The effects of shape on the interaction of colloidal particles. *Ann. N. Y. Acad. Sci.*, 51:627, 1949.

[12] J. A. C. Veerman and D. Frenkel. Phase diagram of a system of hard spherocylinders by computer simulation. *Phys. Rev. A*, 41: 3237, 1990.

[13] S. C. McGrother, D. C. Williamson, and G. Jackson. A re-examination of the phase diagram of hard spherocylinders. *J. Chem. Phys.*, 104:6755, 1996.

[14] P. Bolhuis and D. Frenkel. Tracing the phase boundaries of hard spherocylinders. *J. Chem. Phys.*, 106:666, 1997.

[15] H. Graf and H. Löwen. Density functional theory for hard spherocylinders: phase transitions in the bulk and in the presence of external fields. *J. Phys.: Condens. Matter*, 11:1435, 1999.

[16] J. W. Doane. Polymer dispersed liquid crystals: Boojums at work. *MRS Bull*, XVI:22, 1991.

[17] B. Bahadhur, editor. *Liquid Crystals: Applications and Uses.* World Scientific, Singapore, 1990.

[18] D.-K. Yang, J. L. West, L.-C. Chien, and J. W. Doane. Control of reflectivity and bistability displays using cholesteric liquid crystal. *J. Appl. Phys.*, 76:1331, 1994.

[19] J. W. Doane, N. S. Vaz, B.-G. Wu, and S. Žumer. Field controlled light scattering from nematic microdroplets. *Appl. Phys. Lett.*, 48:269, 1986.

[20] J. L. Fergason. Polymer encapsulated nematic liquid crystals for display and light control applications. *Soc. Inf. Disp. Dig.*, XVI: 68, 1985.

[21] P. S. Drzaic. Polymer dispersed nematic liquid crystal for large area displays and light valves. *J. Appl. Phys.*, 60:2142, 1986.

[22] H. G. Craighead, J. Cheng, and S. Hackwood. New display based on electrically induced index matching in an inhomogeneous medium. *Appl. Phys. Lett.*, 40:22, 1982.

[23] G. P. Crawford, R. Stannarius, and J. W. Doane. Surface induced orientational ordering in the isotropic phase of a liquid crystal material. *Phys. Rev. A*, 44:2558, 1991.

[24] A. Poniewierski and T. J. Sluckin. Theory of the nematic-isotropic transition in a restricted geometry. *Liq. Cryst.*, 2:281, 1987.

[25] A. Golemme, S. Žumer, D. W. Allender, and J. W. Doane. Continuous nematic-isotropic transition in submicron-size liquid-crystal droplets. *Phys. Rev. Lett.*, 61:2937, 1988.

[26] P. Sheng. Boundary-layer phase transition in nematic liquid crystals. *Phys. Rev. A*, 26:1610, 1982.

[27] E. Dubois-Violette and O. Parodi. Emulsions nematiques. effets de champ magnetiques et effets piezoelectriques. *J. de Physique*, 30:C4–57, 1969.

[28] M. J. Press and A. S. Arrot. Theory and experiments on configurations with cylindrical symmetry in liquid-crystal droplets. *Phys. Rev. Lett.*, 33:403, 1974.

[29] S. Candau, P. Le Roy, and F. Debeauvais. Magnetic field effects in nematic and cholesteric droplets suspended in a isotropic liquid. *Mol. Cryst. Liq. Cryst.*, 23:283, 1973.

[30] S. Žumer and J. W. Doane. Light scattering from a small nematic droplet. *Phys. Rev. A*, 34:3373, 1986.

[31] R. D. Williams. Two transitions in tangentially ordered nematic droplets. *J. Phys. A: Math. Gen.*, 19:3211, 1985.

[32] P. S. Drzaic. A new director alignment for droplets of nematic liquid crystal with low bend-to-splay ratio. *Mol. Cryst. Liq. Cryst.*, 154:289, 1987.

[33] G. E. Volovik and O. D. Lavrentovich. Structural transformations in nematic droplets in external electrical field. *Zh. Eksp. Teor. Fiz.*, 85:1997, 1983.

[34] B. Jérôme. Surface effects and anchoring in liquid crystals. *Rep. Prog. Phys.*, 54:391, 1991.

[35] B. Jérôme. *Handbook of Liquid Crystals*, volume 1, page 535. Wiley-VCH, Weinheim, 1998.

[36] G. Barbero and G. Durand. *Liquid Crystals in Complex Geometries*, page 21. Taylor and Francis, London, 1996.

[37] T. Bieker and S. Dietrich. Wetting of curved surfaces. *Physica A*, 252:85, 1997.

[38] M. Dijkstra and R. van Roij. Entropic wetting in colloidal suspensions. *J. Phys.: Condens. Matter*, 17:S3507, 2005.

[39] K. Yaman, M. Jeng, P. Pincus, C. Jeppesen, and C. M. Marques. Rods near curved surfaces and in curved boxes. *Physica A*, 247: 159, 1997.

[40] B. Groh and S. Dietrich. Fluids of rodslike particles near curved surfaces. *Phys. Rev. E*, 59:4216, 1999.

[41] F. C. Frank. I. liquid crystals. on the theory of liquid crystals. *Disc. Faraday Soc.*, 25:19, 1958.

[42] C. W. Oseen. The theory of liquid crystals. *Trans. Faraday Soc.*, 29:883, 1933.

[43] R. L. C. Vink, S. Wolfsheimer, and T. Schilling. Isotropic-nematic interfacial tension of hard and soft rods: application of advanced grand canonical biased sampling techniques. *J. Chem. Phys.*, 123:074901, 2005.

[44] S. Jungblut, R. Tuinier, K. Binder, and T. Schilling. Depletion-induced isotropic-isotropic phase transition in suspensions of rods and spheres. *J. Chem. Phys.*, 127:244909, 2007.

[45] O. Lehmann. Die Hauptsätze der Lehre von den Flussigen Kristallen. In *Flussige Kristalle*. Leipzig, 1904.

[46] R. B. Meyer. Piezoelectric effects in liquid crystals. *Phys. Rev. Lett.*, 22:918, 1969.

[47] N. Metropolis, A. W. Rosenbluth, M. N. Rosenbluth, A. H. Teller, and E. Teller. Equation of state calculations by fast computing machines. *J. Chem. Phys*, 21:1087, 1953.

[48] M. P. Allen and D. J. Tildesley. *Computer Simulation of Liquids*. Oxford University Press, Oxford, England, 1989.

[49] G. Marsaglia. Choosing a point from the surface of a sphere. *Ann. Math. Stat.*, 43:645, 1972.

[50] M. Allen, G. Evans, D. Frenkel, and B. Mulder. *Adv. Chem. Phys.*, LXXXVI:111, 1993.

[51] R. Eppenga and D. Frenkel. Monte carlo study of the isotropic and nematic phases of infinitely thin hard platelets. *Mol. Phys.*, 52:1303, 1984.

[52] Robert J. Low. Measuring order and biaxiality. *Eur. J. Phys.*, 23:111, 2002.

[53] R. L. C. Vink and T. Schilling. Interfacial tension of the isotropic-nematic interface in suspensions of soft spherocylinders. *Phys. Rev. E*, 71:051716, 2005.

[54] S. Chandrasekhar. Surface tension of liquid crystals. *Molecular Crystals*, 2:71, 1966.

[55] W. Huang and G. F. Tuthill. Structure and shape of nematic liquid-crystal droplets. *Phys. Rev. E*, 49:570, 1994.

[56] P. Prinsen and P. van der Schoot. Shape and director-field transformation of tactoids. *Phys. Rev. E*, 68:021701, 2003.

[57] P. Prinsen and P. van der Schoot. Continuous director-field transformation of nematic tactoids. *Eur. Phys. J. E*, 13:35, 2004.

[58] P. Prinsen and P. van der Schoot. Parity breaking in nematic tactoids. *J. Phys.: Condens. Matter*, 16:8835, 2004.

[59] J. H. Erdmann, S. Žumer, and J. W. Doane. Configuration transition in a nematic liquid crystal confined to a small spherical cavity. *Phys. Rev. Lett.*, 64:1907, 1990.

[60] O. O. Prishchepa, A. V. Shabanov, and V. Ya. Zyryanov. Director configurations in nematic droplets with inhomogeneous boundary conditions. *Phys. Rev. E*, 72:031712, 2005.

[61] E. Berggren, C. Zannoni, C. Chiccoli, P. Pasini, and F. Semeria. Computer simulations of nematic droplets with bipolar boundary conditions. *Phys. Rev. E*, 50:2929, 1994.

[62] C. Chiccoli, Y. Lansac, P. Pasini, J. Stelzer, and C. Zannoni. Effect of surface orientation on director configurations in a nematic droplet. a monte carlo. *Mol. Cryst. Liq. Cryst.*, 372:157, 2001.

[63] C. Chiccoli, P. Pasini, I. Feruli, and C. Zannoni. Biaxial nematic droplets and their optical textures. a lattice model computer simulation study. *Mol. Cryst. Liq. Cryst.*, 441:319, 2005.

[64] C. Chiccoli, P. Pasini, F. Semeria, and C. Zannoni. A computer simulation of nematic droplets with radial boundary conditions. *Phys. Lett. A*, 150:311, 1990.

[65] C. Chiccoli, P. Pasini, F. Semeria, and C. Zannoni. Computer simulations of nematic droplets with toroidal boundary conditions. *Mol. Cryst. Liq. Cryst.*, 221:19, 1992.

[66] C. Chiccoli, P. Pasini, F. Semeria, and C. Zannoni. Monte carlo simulations of model nematic droplets. *Mol. Cryst. Liq. Cryst.*, 212:197, 1992.

[67] C. Chiccoli, P. Pasini, F. Semeria, T. J. Sluchin, and C.Zannoni. Monte carlo simulation of the hedgehog defect core in spin systems. *J. Phys. II France*, 5:427, 1995.

[68] E. Berggren, C. Zannoni, C. Chiccoli, P. Pasini, and F. Semeria. Monte carlo study of the molecular organization in the model nematic droplets. field effects. *Chem. Phys. Lett.*, 197:224, 1992.

[69] S. C. McGrother, D. C. Williamson, and G.Jackson. A re-examination of the phase diagram of hard spherocylinders. *J. Chem. Phys.*, 104:6755, 1996.

[70] A. Poniewierski and R. Hołyst. Nematic alignment at a solid substrate: The model of hard spherocylinders near a hard wall. *Phys. Rev. A*, 38:3721, 1988.

[71] R. Hołyst and A. Poniewierski. Nematic-wall surface tension for perfectly aligned hard linear molecules. *Mol. Phys.*, 65:1081, 1988.

[72] R. Hołyst. Exact sum rules and geometrical packing effects in the system of hard rods near a hard wall in three dimensions. *Mol. Phys.*, 68:391, 1989.

[73] A. Poniewierski. Ordering of hard needles at a hard wall. *Phys. Rev. E*, 47:3396, 1993.

[74] M. Dijkstra, R. van Roij, and R. Evans. Wetting and capillary nematization of a hard-rod fluid: A simulation study. *Phys. Rev. E*, 63:051703, 2001.

[75] R. van Roij, M. Dijkstra, and R. Evans. Interfaces, wetting, and capillary nematization of a hard-rod fluid: Theory for the zwanzig model. *J. Chem. Phys.*, 113:7689, 2000.

[76] A. Z. Panagiotopoulos. Direct determination of phase coexistence properties of fluids by monte carlo simulation in a new ensemble. *Mol. Phys.*, 61:813, 1987.

[77] J. Viamontes, P. W. Oakes, and J. X. Tang. Isotropic to nematic liquid crystalline phase transition of f-actin varies from continuous to first order. *Phys. Rev. Lett.*, 118103:97, 2006.

[78] J. D. Bernal and I. Fankuchen. Structure types of protein crystals from virus-infected plants. *Nature (London)*, 139:923, 1937.

[79] J. D. Bernal and I. Frankuchen. X-ray and crystallographic studies of plant virus preparations: I. introduction and preparation of specimens ii. modes of aggregation of the virus particles. *J. Gen. Physiol.*, 25:111, 1941.

[80] Z. Dogic and S. Fraden. Development of model colloidal liquid crystals and the kinetics of the isotropic-smectic transition. *Philos. Trans. R. Soc. London, Ser. A*, 359:997, 2001.

[81] P. W. Oakes, J. Viamontes, and J. X. Tang. Growth of tactoidal droplets during the first-order isotropic to nematic phase transition of f-actin. *Phys. Rev. E*, 75:061902, 2007.

[82] A. V. Kaznacheev, M. M. Bogdanov, and A. S. Sonin. The influence of anchoring energy on the prolate shape of tactoids in lyotropic inorganic liquid crystals. *J. Exp. Theor. Phys.*, 97: 1159, 2003.

[83] M. C. Mourad, E. J. Devid, M. M. van Schooneveld, C. Vonk, and M. N. W. Lekkerkerker. Formation of nematic liquid crystals of sterically stabilized layered double hydroxide platelets. *J. Chem. Phys. B*, 112:10142–52, 2008.

[84] A. Kaznacheev, M. M. Bogdanov, and S. A. Taraskin. The nature of prolate shape of tactoids in lyotropic inorganic liquid crystals. *J. Exp. Theor. Phys.*, 95:57, 2002.

[85] A. Cuetos and M. Dijkstra. Kinetic pathways for the isotropic-nematic phase transition in a system of colloidal hard rods: A simulation study. *Phys. Rev. Lett.*, 98:095701, 2007.

[86] R. Berardi, A. Costantini, L. Muccioli, S. Orlandi, and C. Zannoni. A computer simulation study of the formation of liquid crystal nanodroplets from a homogeneous solution. *J. Chem. Phys.*, 126:044905, 2007.

[87] M. A. Bates. Computer simulation studies of nematic liquid crystal tactoids. *Chem. Phys. Lett.*, 368:87, 2003.

[88] F. Oosawa and S. Asakura. On interaction between two bodies immersed in a solution of macromolecules. *J. Chem. Phys.*, 22: 1255, 1954.

[89] A. Vrij. Polymers at interfaces and the interactions in colloidal dispersions. *Pure Appl. Chem.*, 48:471, 1976.

[90] H. Lekkerkerker, W. Poon, P. Pusey, A. Stroobants, and P. Warren. Phase behaviour of colloid + polymer mixtures. *Europhys. Lett.*, 20:559, 1992.

[91] H. Lekkerkerker and A. Stroobants. Phase behaviour of rod-like colloid + flexible polymer mixtures. *Nuovo Cimento D*, 16:949, 1994.

[92] J. Buitenhuis, L. N. Donselaar, P. A. Buining, A. Stroobants, and H. N. W. Lekkerkerker. Phase separation of mixtures of colloidal boehmite rods and flexible polymer. *J. Colloid Interface Sci.*, 175:46, 1995.

[93] H. Wang, W. Zhou, D. L. Ho, K. I. Winey, J. E. Fischer, C. J. Glinka, and E. K. Hobbie. Dispersing single-walled carbon nanotubes with surfactant: A small angle neutron scattering study. *Nanoletters*, 4:1789, 2004.

[94] P. G. Bolhuis, A. Stroobants, D. Frenkel, and H. N. W. Lekkerkerker. Numerical study of the phase behaviour of rodlike colloids with attractive interactions. *J. Chem. Phys.*, 107:1551, 1997.

[95] S. V. Savenko and M. Dijkstra. Phase behavior of a suspension of colloidal hard rods and nonadsorbing polymer. *J. Chem. Phys.*, 124:234902, 2006.

[96] M. Gruenwald, E. Rabane, and C. Dellago. Mechanisms of the wurtzite to rocksalt transformation in cdse nanocrystals. *Phys. Rev. Lett.*, 96:255701, 2007.

[97] M. Gruenwald and C. Dellago. Ideal gas pressure bath: a method for applying hydrostatic pressure in the computer simulation of nanoparticles. *Mol. Phys.*, 104:3709, 2006.

[98] S. Jungblut. *unpublished.*

[99] R. van Roij. The isotropic and nematic liquid crystal phase of colloidal rods. *Eur. J. Phys.*, 26:S57, 2005.

[100] M. Gruenwald, C. Dellago, and Ph. L. Geissler. An efficient transition path sampling algorithm for nanoparticles under pressure. *J. Chem. Phys.*, 127:154718, 2007.

[101] A. Cuetos, B. Martinez-Haya, and S. Lago. Use of parsons-lee and onsager theories to predict nematic and demixing behavior in binary mixtures of hard rods and hard spheres. *Phys. Rev. E*, 75:061701, 2007.

[102] P. van der Schoot. Remarks on the interfacial tension in colloidal systems. *J. Phys. Chem. B*, 103:8804, 1999.

[103] A. Rapini and M. Papoular. Distorsion d'une lamelle nématique sous champ magnétique conditions d'ancrage aux parois. *J. Phys. (Paris) Colloq.*, 30:C4–54, 1969.

[104] A. Cuetos, R. van Roij, and M. Dijkstra. Isotropic-to-nematic nucleation in suspensions of colloidal rods. *Soft Matter*, 4:757, 2008.

[105] J. Nehring and A. Saupe. On the elastic theory of uniaxial liquid crystals. *J. Chem. Phys.*, 54:337, 1971.

[106] S.-D. Lee and R. B. Meyer. Computations of the phase equilibrium, elastic constants, and viscosities of a hard-rod nematic liquid crystal. *J. Chem. Phys.*, 84:3443, 1986.

[107] G. J. Vroege and T. Odijk. Elastic moduli of a nematic liquid-crystalline solution of polyelectrolytes. *J. Chem. Phys.*, 87:4223, 1987.

[108] B. Tjipto-Margo, G. T. Evans, M. P. Allen, and D. Frenkel. Elastic constants of hard and soft nematic liquid crystals. *J. Phys. Chem.*, 96:3942, 1992.

[109] G. J. Vroege and H. Lekkerkerker. Phase transitions in lyotropic colloidal and polymer liquid crystals. *Rep. Progr. Phys.*, 55:1241, 1992.

[110] S. Lee. A numerical investigation of nematic ordering based on a simple hard-rod model. *J. Chem. Phys.*, 87:4972, 1987.

Acknowledgments

I would like to express my gratitude to all the people I met during the years of my Ph.D. I have gained something from all of you. I thank my thesis advisors for giving me an opportunity to work on these exciting projects and for giving me the scientific background a very clear way. Furthermore, I appreciate a lot the fact of giving me enough time for finishing my thesis.

I thank all the people in our scientific group for the pleasant atmosphere, interesting conversations, and a lot of help with my work.

Finally, I thank my friends, my sister, and especially my parents for their great support during my whole life.